Research Square

Preprints are preliminary reports that have not undergone peer review.
They should not be considered conclusive, used to inform clinical practice,
or referenced by the media as validated information.

An updated spatio-temporal assessment of climate dynamics in semi-arid Central Asia: The evidence from the Eastern Kazakhstan

Aidos Omarov[1]
Kazakhstan
Amanzhol Kuderin[2]
Kazakhstan
Zhumakhan Mustafayev[2]
Kazakhstan
Irina Skorintseva[2]
Kazakhstan
Marat Karatayev[3]
marat.karatayev@uni-graz.at
Kazakhstan

Research Article

Keywords: climate change, climatic exposure, homogeneity testing, Mann–Kendall, SPEI, potential evapotranspiration, semi-arid Central Asia, Abai Region, ERA5-Land, Kazakhstan

Posted Date: November 25th, 2026

DOI: https://doi.org/10.21203/rs.3.rs-11681279/v1

License: This work is licensed under a Creative Commons Attribution 4.0 International License.
Read Full License

Additional Declarations: No competing interests reported.

An updated spatio-temporal assessment of climate dynamics in semi-arid Central Asia: The evidence from the Eastern Kazakhstan

Aidos Omarov[1], Amanzhol Kuderin[2], Zhumakhan Mustafayev[2], Irina Skorintseva[2], Marat Karatayev[3]*

[1]Al-Farabi Kazakh National University, School of Geography and Environmental Management, Al-Farabi Ave. 70, A15E3C7, Almaty, Kazakhstan; [2]Institute of Geography and Water Security, Department of Landscape Study and Problems of Nature Management, Seifullin Str., 458/1, Almaty 050000, Kazakhstan; [3]Institute of Environmental Systems Sciences, Karl-Franzens University of Graz, Merangasse 18-1, A-8010, Graz, Austria;
*Corresponding author: marat.karatayev@uni-graz.at

Abstract

This paper analyzes monthly air temperature, humidity and precipitation from 15 stations of national hydrometeorological service of the Republic of Kazakhstan (Kazhydromet) in the Abai Region of Eastern Kazakhstan. The data were checked for quality and consistency using SNHT and Pettitt tests. Climate trends were analyzed using Sen's slope and the Mann–Kendall test, with adjustments to reduce false results across stations. Climate anomalies were compared with the World Meteorological Organization (WMO) reference period of 1991–2020. Potential evapotranspiration was estimated using four methods: Thornthwaite, Hargreaves-Samani, Penman–Monteith, and an adjusted Thornthwaite method (TH-adj.) calibrated to the Penman–Monteith level, the aridity index and SPEI/SPI were computed. The average annual temperature increased by +0.41 °C per decade (95% CI 0.29–0.55; +2.4 °C over 1966–2025) with a step change in 1989 (+1.2 °C); all 15 stations warmed significantly ($q < 0.003$), and station-to-station differences in warming rate (0.21–0.53 °C per decade) were largely artefacts of six inhomogeneous records (0.38–0.43 °C per decade after adjustment). Spring season experienced the fastest warming, with temperatures increasing by 0.61 °C per decade. Precipitation showed no significant increase or decrease with variability (Levene test, $p = 0.42$). Rising temperature-based evaporative demand (+13 to +19 mm per decade regionally and positive at all stations; the short Penman–Monteith record shows a smaller, non-significant increase) nevertheless reduced the climatic water balance (-10 to -17 mm per decade) and produced significant drying in spring and the April–September growing season (SPEI-6 -0.18 to -0.21 per decade; SPI-6 no trend), while the share of station-months in moderate drought rose 1.9-fold after 1991 (regional drought episodes: three in 1967–1990, four in 1991–2025). Relative humidity declined in spring (-0.78 percentage points per decade) but its station trends are sensitive to instrument-related breaks around 1996-1998 and 2005-2006. Temperature trends showed no elevation control within 148–842 m. ERA5-Land monthly fields for 1991-2020 were validated against the 15 stations ($r = 0.93$ for annual temperature, mean bias +0.6 °C; precipitation overestimated by about 30%) and, after bias correction, used only as a supplement to describe the uplands above the station elevation range (all trend, PET, SPEI and correlation results rest on station data alone): mean annual temperature falls to about 1.4 °C and precipitation rises to about 470 mm in cells above 1,200 m, whereas the reanalysis temperature trend (+0.41 °C per decade in 1991–2020) is about twice the station value (+0.19) and was not used for inference. The results indicate that climatic exposure of pastures (87% of agricultural land) and rain-fed crops is rising in spring and early summer through thermally driven drying rather than through changes in precipitation, and we show why trend fields from 15 stations should be presented as station values rather than interpolated surfaces.

Keywords: climate change; climatic exposure; homogeneity testing; Mann–Kendall; SPEI; potential evapotranspiration; semi-arid Central Asia; Abai Region; ERA5-Land; Kazakhstan

Graphical abstract

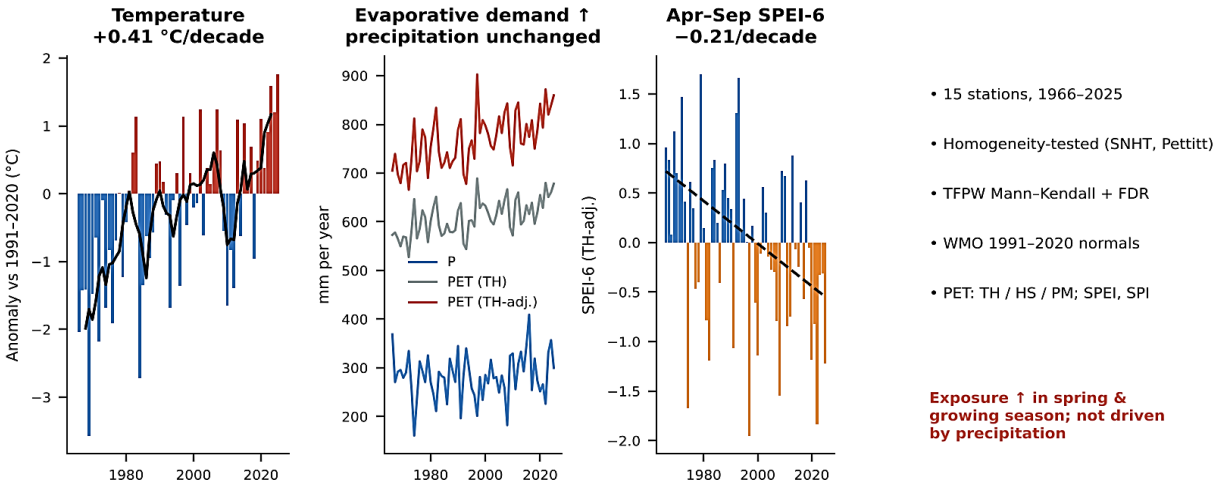

Graphical abstract: robust warming and rising evaporative demand with unchanged precipitation produce spring and growing-season drying (SPEI-6) in the Abai Region, 1966–2025.

1. Introduction

Climate change has emerged as one of the most profound environmental challenges of the twenty-first century, altering temperature regimes, precipitation patterns, atmospheric moisture conditions, and hydrological processes across diverse climatic regions worldwide. These transformations are primarily driven by anthropogenic greenhouse gas emissions, land-use changes, and complex feedback mechanisms within the Earth's climate system, resulting in unprecedented rates of environmental change and increasing climate-related risks (Chen et al., 2011; Intergovernmental Panel on Climate Change [IPCC], 2023b; Masson-Delmotte, 2024). Although global warming is unequivocal, its impacts are expressed unevenly across regions due to variations in geographical setting, topography, atmospheric circulation, and land–atmosphere interactions (Magnan et al., 2021; Pongratz et al., 2021). Consequently, regional-scale assessments have become increasingly important for understanding local manifestations of climate change and informing evidence-based adaptation strategies.

Among the world's most climate-sensitive regions, Central Asia has been identified as a climate change hotspot characterized by accelerated warming, increasing hydroclimatic variability, and growing environmental vulnerability (IPCC, 2023a; Lioubimtseva & Henebry, 2009). The region's predominantly arid and semi-arid landscapes are particularly susceptible to climatic perturbations because ecological productivity, agricultural systems, and water resources are strongly dependent on limited and highly variable moisture availability. Recent studies indicate that warming rates across Central Asia exceed the global average, while changes in precipitation and atmospheric moisture exhibit considerable spatial and temporal heterogeneity, creating substantial uncertainty regarding future hydroclimatic conditions (Haag et al., 2019; Yao et al., 2022). These evolving patterns have intensified concerns regarding drought occurrence, land degradation, water security, and ecosystem resilience throughout the region.

Kazakhstan occupies a strategically important position within the continental interior of Eurasia, at the intersection of Siberian, Central Asian, and European atmospheric circulation systems, which makes it responsive to large-scale oscillations such as the Siberian High and North Atlantic circulation (Gong & Ho, 2002; Schiemann et al., 2008). Numerous studies have documented significant warming across Kazakhstan, accompanied by increasing climatic variability and heightened risks of drought and water stress (Karatayev et al., 2022; Salnikov et al., 2023). However, most assessments rely on national-scale analyses, coarse gridded datasets, or short observational periods that cannot capture local heterogeneity (Hu et al., 2014; Hu et al., 2017), and station-based studies seldom report whether their records are homogeneous, whether serial correlation was accounted for before trend testing, or whether the multiplicity of station-wise tests was controlled.

The need for updated assessments is particularly urgent in Eastern Kazakhstan. The Abai Region, established in 2022, encompasses lowland steppe, the upland landscapes of the Kazakh Uplands (Saryarka), and the foothills of the Tarbagatai system, and it remains underrepresented in the international literature (Chernykh et al., 2025; Rakhimova et al., 2020; Vakulchuk et al., 2023; Yapiyev et al., 2025). Furthermore, most climate studies in Central Asia have focused on temperature, whereas relative humidity and evaporative demand have received less attention (Chen et al., 2016; Karthe et al., 2015; Tabari et al., 2011). Recent SPI- and SPEI-based assessments for Kazakhstan (Bissenbayeva et al., 2025; Ryssaliyeva et al., 2025) are regional or national in scope and, to our knowledge, none combines homogeneity-tested station records with a bracket of PET formulations for the Abai Region. Statements about "increasing water deficit" or "drought risk" in the region are frequently made from temperature and precipitation alone, without potential evapotranspiration (PET) or a standardized drought index, although the choice of PET formulation can change drought trends substantially (Dai, 2013; Sheffield et al., 2012; Vicente-Serrano et al., 2010).

Three methodological issues motivate this study. First, trends from a small station network are sensitive to undetected inhomogeneities, which can inflate or mask spatial differences in warming (Menne et al., 2009; Venema et al., 2012). Second, the choice of climatological reference period affects the magnitude and interpretation of calculated anomalies and their comparability across studies. We therefore use the WMO standard normal period of 1991–2020 to provide a consistent reference for assessing recent and long-term climate variability (World Meteorological Organization [WMO], 2017). Third, spatially interpolated trend maps imply spatial structure that sparse networks may not contain (Hengl et al., 2007; Li & Heap, 2014). We therefore ask: (Q1) Is the warming of the Abai Region robust to inhomogeneity and serial correlation, and do stations differ in their warming rates? (Q2) Which seasons carry the signal? (Q3) Do changes in precipitation, atmospheric humidity and evaporative demand support the widely repeated claim of an increasing climatic water deficit, and at what time scale? (Q4) Has the variability of anomalies increased? (Q5) How spatially coherent are the climate fields, and does relief or latitude control means and trends within the elevation range sampled by the network?

To answer these questions we combine 60 years (1966–2025) of monthly air temperature, relative humidity and precipitation from 15 stations with a documented quality-control and homogeneity workflow, trend-free pre-whitened Mann–Kendall tests with false-discovery-rate control, WMO-normal anomalies, three PET formulations, the aridity index, SPEI and SPI at 3–12-month scales, detrended correlation analysis, and cross-validated tests of interpolation skill. The study assesses climatic exposure and hydroclimatic change; it does not quantify vulnerability, which additionally requires sensitivity and adaptive-capacity indicators beyond the scope of meteorological records (IPCC, 2023a).

The contribution of this study lies in the integrated assessment of long-term climate change and climatic water-balance conditions across a sparsely monitored semi-arid region. Rather than relying on trend estimates alone, the analysis examines the sensitivity of climate-trend inference to observational inhomogeneities, serial correlation, and multiple testing, while comparing drought-related indicators derived using alternative potential evapotranspiration formulations. The study further evaluates whether the available station network supports reliable spatial representation of climate

variables and whether elevation and latitude help explain the observed spatial patterns. By applying these complementary assessments to a consistent 60-year observational period, the study aims to distinguish robust regional signals from findings that are more dependent on methodological choices or local station characteristics. Because the stations sample only 148–842 m, ERA5-Land (Muñoz-Sabater et al., 2021) is used only as a supplement: after validation against the stations it describes the climate of the uplands that the network does not reach, whereas all trend, PET, SPEI, correlation and interpolation results rest on station data alone.

2. Study area, data and methods

2.1 Study area

The Abai Region of Kazakhstan (formerly part of the East Kazakhstan Region) lies between approximately 46.65° N and 50.87° N and 77.0° E and 82.8° E (Fig. 1). It borders Russia (Altai Krai) to the north and China (Xinjiang Uyghur Autonomous Region) to the southeast and is flanked by the Zhetysu, Karaganda and Pavlodar regions to the west. The central and northern parts are dominated by the Kazakh Uplands (Saryarka), a dissected peneplain with typical elevations of 500–700 m a.s.l. To the north the terrain passes into the southern margin of the West Siberian Plain, with lowlands below 200 m (Semey, Semyarka). The southeastern sector is defined by the Tarbagatai Range, which rises to approximately 3,000 m and forms the orographic barrier between the Zaisan Depression and the Balkhash–Alakol basin. Altitudinal and geomorphological heterogeneity generates gradients in temperature, humidity and precipitation (Aizen et al., 1997; Gnann et al., 2025; Li et al., 2022; Löffler et al., 2006), and the interaction of orography with westerly advection, Siberian anticyclones and dry Central Asian air masses makes the region sensitive to climate variability (Karatayev et al., 2022).

The region hosts 594.3 thousand inhabitants, 37.0% of them rural (Bureau of National Statistics of the Agency for Strategic Planning and Reforms of the Republic of Kazakhstan [BNS], 2025). Primary production accounts for 61.8% of the 3.93 trillion KZT Gross Regional Product. Of 18.57 million ha, 9.10 million ha are agricultural land, dominated by pastures (7.94 million ha; 87.2%), with arable land (806.7 thousand ha) and hayfields (247.3 thousand ha) (Committee for Land Resources Management of the Ministry of Agriculture of the Republic of Kazakhstan [CLRM], 2025). Pasture productivity, livestock carrying capacity and rain-fed crop yields therefore depend directly on spring and early-summer moisture, which motivates the seasonal focus of this study.

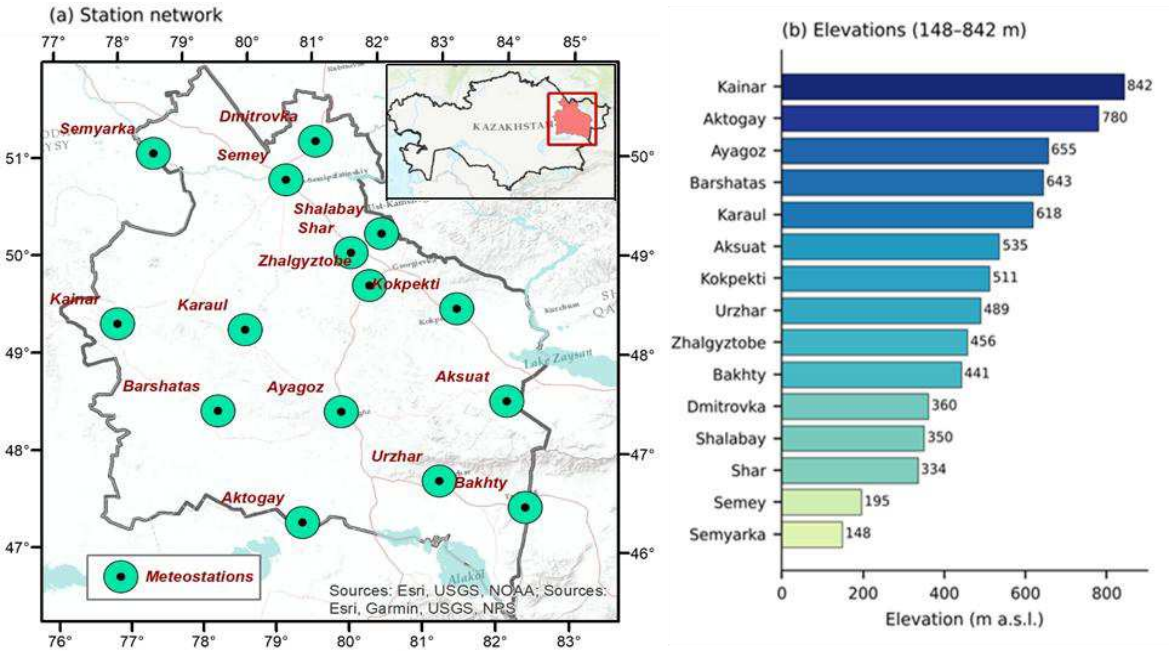

Fig. 1. Study area. (a) The 15 meteorological stations, with the location of the study area within Kazakhstan (inset); country outlines from ESRI. (b) Station elevations (148–842 m a.s.l.). The Tarbagatai Range (up to ≈3000 m) is not sampled by any station.

2.2 Meteorological data, quality control and homogeneity assessment

Monthly series of mean air temperature (°C), mean relative humidity (%) and precipitation totals (mm) for 1966–2025 were compiled for 15 stations of the RSE "Kazhydromet" national network (Table 1). For 2001–2024 the Kazhydromet database additionally provides monthly mean daily maximum and minimum temperature and wind speed, used only for PET (Section 2.4). The records comprise 10,800 station-months (15 stations × 60 years × 12 months); 32 temperature, 53 precipitation and 992 humidity values are missing (including station-months that are absent altogether from the source tables, not only empty cells), almost all humidity gaps belonging to 1966–1976 at six stations (Aktogay, Barshatas, Bakhty, Dmitrovka, Zhalgyztobe, Semey), whose humidity records begin in 1977 with 7–8 valid months. Humidity was therefore analysed for the common period 1978–2025 (48 years); the first annual value at the six stations is 1978. Thirty-two further values carry the source flag "H" (incomplete data; temperature 3, humidity 29) and were

excluded rather than used as numbers; their inclusion changes Sen slopes by ≤ 0.001 °C yr^{-1} and ≤ 0.004 % yr^{-1} and does not alter significance.

Screening comprised: (I) physical-range checks (RH > 100% or < 5%, P < 0, T outside −55…+45 °C), none failing; (II) detection of duplicated blocks of ≥ 6 identical months, none found; (III) a robust standard score (median and MAD of each station–calendar month) with |z| > 5 flagging 51 extreme monthly values (one temperature value, January 1969, −27.2 °C; 50 precipitation totals; no humidity values), all judged physically plausible (cold-air outbreaks, convective or heavy-snow months) and retained; and (IV) removal of one physically impossible wind-speed value (Ayagoz, December 2024, 2025 m s^{-1}). No other observation was removed or infilled in the main analysis.

Annual temperature and humidity were computed as the mean of monthly anomalies relative to each station's monthly climatology (1966–2025) plus its climatological annual mean, which prevents a missing cold month from biasing the annual mean; years with fewer than 10 valid months were set to missing (temperature 5 station-years, humidity 8). Annual precipitation is the sum of 12 monthly totals; incomplete years (31 of 900 station-years, 3.4%) were not infilled, and a sensitivity run infilling the 21 years with a single missing month by the climatological month-share method changed no station slope by more than 0.21 mm yr^{-1} and no significance class. Seasons are DJF (December of the preceding year plus January and February; first DJF 1967), MAM, JJA and SON; temperature and humidity seasons require ≥ 2 of 3 months and precipitation seasons all 3 months.

Table 1. Meteorological stations, start of the humidity record, break years detected by the homogeneity tests.

Station	Lat (°N)	Lon (°E)	Elev. (m)	Physiographic zone	RH record starts	Break T	Break RH	Break P
Kainar	49.200	77.367	842	Foothill-steppe (Saryarka)	1966	2014	–	2009
Aktogay	47.000	77.000	780	Foothill plain	1977	–	–	–
Ayagoz	47.967	80.450	655	Steppe plain	1966	2005	–	–
Barshatas	48.170	78.670	643	Upland steppe	1977	–	2005	–
Karaul	49.000	79.333	618	Steppe	1966	2009	–	–
Aksuat	47.767	82.817	535	Semi-arid steppe	1966	1989	–	–
Kokpekti	48.750	82.301	511	Steppe plain	1966	2006	2006	–
Urzhar	47.117	81.617	489	Steppe (Tarbagatai foothills)	1966	2001	1997	–
Zhalgyztobe	49.217	81.217	456	Steppe	1977	–	1998	–
Bakhty	46.650	82.750	441	Semi-arid (Balkhash–Alakol basin)	1977	–	2012	–
Dmitrovka	50.770	80.830	360	West Siberian plain margin	1977	–	1996	–
Shalabay	49.700	81.510	350	Steppe lowland	1966	–	–	–
Shar	49.580	81.050	334	Steppe lowland	1966	–	1998	–
Semey	50.417	80.300	195	Lowland steppe (Irtysh valley)	1977	–	–	–
Semyarka	50.867	78.350	148	West Siberian lowland	1966	–	–	–

Absolute homogeneity tests confound genuine climate trends with breaks, so relative tests were applied to the difference between each station and the mean of the other 14 stations (log-ratio for precipitation). The reference series correlate strongly with the candidate series for temperature (r = 0.88–0.98) and moderately for precipitation (0.47–0.78) and humidity (0.19–0.73), which limits detection power for the latter two. We applied the Standard Normal Homogeneity Test (SNHT; Alexandersson, 1986), whose statistic for a series of standardized values z of length n is

$$T(k) = k\bar{z}_{1:k}^2 + (n-k)\bar{z}_{k+1:n}^2$$
$$T_{\max} = \max_{1 \le k < n} T(k) \quad (1)$$

where $\bar{z}_1$ and $\bar{z}_2$ are the means before and after position k, with the p-value obtained by Monte Carlo simulation (20,000 series), and the non-parametric Pettitt test (Pettitt, 1979). A series was flagged as having a candidate break only if SNHT p < 0.01, Pettitt p < 0.05 and the two break years differed by ≤ 5 years. Because station metadata (relocations, instrument changes) were not available, breaks are "candidate" breaks. For temperature, the part of the record before the break was shifted by the estimated step (mean after minus mean before in the difference series) to build an "adjusted" series; this is reported strictly as a sensitivity analysis, no value was removed, and adjusted and unadjusted results are shown side by side. Humidity and precipitation were not adjusted; flagged series are identified in every table and interpreted with caution.

2.3 Climate normals, anomalies and trend analysis

Anomalies were referenced to the WMO standard normal of 1991–2020 (WMO, 2017) (the 1961–1990 normal is unavailable because records start in 1966). Monthly normals were computed per station; every station–month has at least 28 of 30 valid years for temperature and precipitation and at least 26 for humidity, exceeding the WMO threshold of 24 years. For month m of year i, the anomaly is

$$A_{i,m} = X_{i,m} - \overline{X}_{m,1991-2020} \quad (2)$$

and annual temperature and humidity anomalies are means of the monthly anomalies (≥ 10 months), whereas precipitation anomalies are the annual total minus the annual normal, also expressed as a percentage of the normal. Regional temperature and humidity series are means of the 15 stations; regional precipitation, PET and water-balance

series are means of station anomalies added to the network-mean climatology, so that years with a missing station do not bias the regional level (≥ 12 stations required in both cases). Changing the baseline shifts anomalies by a constant and leaves trends unchanged. To test the claim of increasing anomaly amplitude we compared the standard deviation of regional anomalies between 1966–1990 and 1991–2025 with Levene's test (median-centred) on series detrended within each period (Levene, 1960), tested station-wise with FDR control, computed the Sen slope of the absolute standardized anomaly, and counted anomalous years ($|z| \geq 1$, with z standardized by the 1991–2020 standard deviation).

Trends were estimated for annual and seasonal series of every station and for regional means. The magnitude was quantified with Sen's slope (Sen, 1968),

$$\beta = \text{median}\left(\frac{x_j - x_i}{j - i}\right), \quad j > i \tag{3}$$

with 95% confidence limits from the Theil–Sen interval for stations and a moving-block bootstrap (Künsch, 1989) for the regional temperature trend; total change is β times the span between the first and the last year (59 years for 1966–2025). Significance was tested with the Mann–Kendall test (Mann, 1945; Yue et al., 2002) based on

$$S = \sum_{k=1}^{n-1} \sum_{j=k+1}^{n} \text{sgn}\,(x_j - x_k)$$

$$\text{Var}(S) = \frac{n(n-1)(2n+5) - \sum_{p=1}^{g} t_p\,(t_p - 1)(2t_p + 5)}{18}$$

$$Z = \begin{cases} \frac{S-1}{\sqrt{\text{Var}(S)}}, & S > 0 \\ 0, & S = 0 \\ \frac{S+1}{\sqrt{\text{Var}(S)}}, & S < 0 \end{cases} \tag{4}$$

where t_p is the size of tied group p. Because serial correlation inflates the false-positive rate, the lag-1 autocorrelation r_1 of the Sen-detrended series was tested against ±1.96/√n (lags 1–5 inspected); when significant, trend-free pre-whitening (TFPW) was applied before the test (Künsch, 1989):

$$\begin{aligned} x'_t &= x_t - \beta t \\ y_t &= x'_t - r_1 x'_{t-1} \\ x''_t &= y_t + \beta t \end{aligned} \tag{5}$$

and the Mann–Kendall test applied to x''; otherwise the standard test was used. This TFPW-based p-value is the primary result. The Hamed–Rao variance correction (Hamed & Rao, 1998; Hamed, 2008) was computed as a sensitivity analysis only, because its correction factor was unstable (below 0.5 or above 2 in 55 of 240 cases) and it inflated the number of "significant" stations. Because 15 stations are tested per variable and season, the Benjamini–Hochberg procedure (Benjamini & Hochberg, 1995) was applied within each variable–season, and a station trend is called significant if q < 0.05 (q ≤ 0.10 corresponds to the global criterion of Wilks (2016)). A step change in the regional temperature series was located with the Pettitt test. Humidity trends cover 1978–2025.

2.4 Potential evapotranspiration, climatic water balance and drought indices

PET was estimated by three methods. The Thornthwaite method (TH; Thornthwaite, 1948), using monthly mean temperature, latitude-dependent day length and a heat index fixed from the station climatology, is the only method that covers 1966–2025. The Hargreaves–Samani method (HS; Hargreaves & Samani, 1985) and the FAO-56 Penman–Monteith method (PM; Allen et al., 1998) with the limited-data options (radiation from the temperature range, vapour pressure from relative humidity, wind speed converted to 2 m assuming a 10 m measurement height) were computed for 2001–2024, when daily extreme temperatures and wind are available. TH underestimates PM by about 27% in this overlap, so a second series, "TH-adj." PET (Thornthwaite adjusted to the Penman–Monteith level), was created by scaling TH with station- and month-specific factors from the overlap,

$$\begin{aligned} \text{PET}_{\text{TH-adj}}(s,m,t) &= f_{s,m}\text{PET}_{\text{TH}}(s,m,t) \\ \text{f}_{\text{s,m}} &= \frac{\overline{\text{PET}}_{\text{PM,s,m}}}{\overline{\text{PET}}_{\text{TH,s,m}}} \end{aligned} \tag{6}$$

(2001–2024; f = 1 where mean PET_{TH} < 10 mm), which preserves the temperature-driven variability of TH while correcting its seasonal level. Because the factors are fitted for 2001–2024 and applied unchanged to 1966–2000, $TH - adj.$ is a level-adjusted Thornthwaite series, not a Penman–Monteith reconstruction; the two series share their variability and are not independent estimates. The climatic water balance is

$$\begin{aligned} D &= P - \text{PET} \\ AI &= \frac{P}{\text{PET}}, \end{aligned} \tag{7}$$

with aridity classes of UNEP (Middleton & Thomas, 1997). The Standardized Precipitation Evapotranspiration Index (SPEI; Beguería et al., 2014; Vicente-Serrano et al., 2010) was computed from monthly D accumulated over 3, 6 and 12 months, fitting a generalised logistic distribution by L-moments (Hosking, 1990) separately for each calendar month over 1966–2025 and transforming to standard normal; the SPI (McKee et al., 1993) used a zero-inflated gamma distribution for P alone. SPEI-3 ending in February, May, August and November represents DJF, MAM, JJA and SON, SPEI-6 ending in September the April–September growing season, and SPEI-12 ending in December the calendar year. Fitted indices have a mean ≈ 0 and a standard deviation of 0.99–1.01 for every calendar month. Regional droughts were defined as regional-mean SPEI-12 ≤ −1 for ≥ 3 consecutive months (severity = sum of |SPEI|); because a regional criterion is rarely met, the share of station-months below −1, −1.5 and −2 was compared between 1967–1990 and 1991–2025. Trends of indices follow Section 2.3 and cover 1967–2025.

2.5 Relationships, spatial structure and interpolation skill

Relationships among regional annual and seasonal series were quantified with Pearson correlations after removing a linear trend from both series, so that shared trends do not generate spurious correlation. Serial correlation was handled by the effective sample size (Bretherton et al., 1999)

$$n_{\text{eff}} = n\frac{1-r_{1x}r_{1y}}{1+r_{1x}r_{1y}} \tag{8}$$

used in the t-test, with FDR control within each family of tests. Station-wise correlations were counted to judge whether a relationship is regional or station-specific. Pairs sharing a component by construction (for example P and P − PET, or SPEI and SPI) are called structural and are not interpreted as independent evidence.

Spatial coherence was assessed with detrended correlations for the 105 station pairs fitted by $r = exp(-d/L)$, with the decorrelation length L estimated by least squares (reported only where it is identifiable within the 569 km extent of the network) and its standard error by leave-one-station-out jackknife, and with a partial Mantel test (Mantel, 1967) of whether elevation differences reduce correlation after accounting for distance (2,000 permutations). Dependence of 1991–2020 means on geography was tested by OLS on elevation and latitude (n = 15, df = 12, 95% CI of coefficients) and by Spearman rank correlations, with FDR control. Skill of spatial interpolation was evaluated by leave-one-out cross-validation (LOOCV) of five predictors: the constant station mean, inverse-distance weighting, OLS on elevation and latitude, ordinary kriging with a fitted parametric variogram, and regression kriging (OLS on elevation and latitude plus ordinary kriging of residuals) (Hengl et al., 2007),

$$\text{Skill} = 1 - \frac{\text{MSE}_{\text{method}}}{\text{MSE}_{\text{constant mean}}} \tag{9}$$

for the mean annual temperature field and for the fields of trend magnitudes. Station elevation was used as the only relief covariate because the network spans 148–842 m and a digital elevation model would not add information at station points; the uplands are treated separately with ERA5-Land (Section 2.6). Trend values are therefore presented as station symbols (Fig. 7) instead of interpolated surfaces unless a predictor shows positive skill. All computations were done in Python (NumPy, SciPy, pandas); Fig. 2 summarizes the workflow.

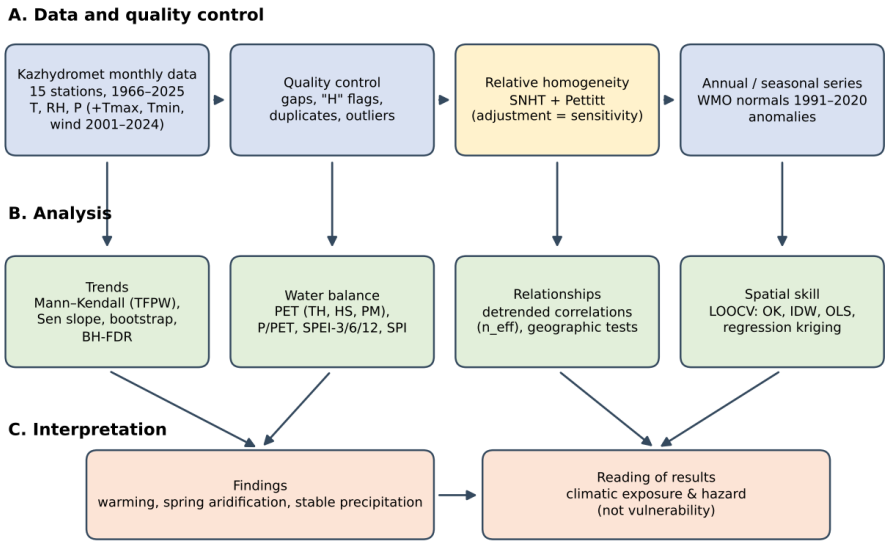

Fig. 2. Analytical workflow. Yellow: homogeneity testing, whose adjustment is reported only as a sensitivity analysis. TH, HS, PM = Thornthwaite, Hargreaves–Samani, Penman–Monteith; LOOCV = leave-one-out cross-validation; OK = ordinary kriging; IDW = inverse-distance weighting.

2.6 ERA5-Land reanalysis for the unsampled uplands

ERA5-Land was used only to supplement station observations in unsampled uplands; all trend, PET, SPEI, correlation and interpolation analyses were based exclusively on station data. Monthly 1991–2020 fields of 2 m air temperature, total precipitation and total evaporation were obtained at 0.1° (≈9 km) resolution from the Copernicus Climate Data Store. Precipitation and evaporation, supplied as daily means in metres, were converted to monthly totals in mm by multiplying by the number of days and by 1,000; evaporation signs were reversed. The 2,282 grid cells within the regional boundary were retained, regional means were area-weighted by the cosine of latitude, and values were bilinearly interpolated to station coordinates. Cell-mean elevation was derived from a 1-arcsecond DEM.

ERA5-Land (Muñoz-Sabater et al., 2021) was evaluated against the 15 stations for 1991–2020 using Pearson correlations and mean bias for annual and seasonal series. Temperature bias was also assessed after accounting for station–grid elevation differences using the regional ERA5-Land lapse rate (−3.1 °C km^{-1}). A single regional additive correction was applied to temperature and a multiplicative correction, based on the median reanalysis-to-station mean ratio, to precipitation. Correction performance was evaluated by leave-one-station-out cross-validation, and corrected fields were summarised across six elevation belts. Reanalysis trends were estimated using the Theil–Sen slope and Mann–Kendall test and compared with, but did not replace, station-based trends. Because station elevations range from 148 to 842 m, corrected estimates above this range remain extrapolations. Total evaporation was extracted but not validated or interpreted.

3. Results

3.1 Data completeness and detection of inhomogeneities in observational series

Completeness is high for temperature (99.7% of monthly values) and precipitation (99.5%), and the exclusion of incomplete years removed only 5 of 900 station-years for temperature, 8 of 720 for humidity (1978–2025) and 31 of 900 (3.4%) for precipitation (Table 2). The relative homogeneity tests flagged six temperature series, seven humidity series and one precipitation series (Table 3, Fig. 3). Temperature breaks have magnitudes of −0.83 to +0.53 °C and are of both signs: three upward (Kokpekti 2006, +0.53 °C; Ayagoz 2005, +0.40 °C; Aksuat 1989, +0.35 °C) and three downward (Urzhar 2001, −0.83 °C; Karaul 2009, −0.33 °C; Kainar 2014, −0.32 °C). Humidity breaks are larger (1.8–6.9 percentage points) and cluster in 1996–1998 (Dmitrovka, Urzhar, Zhalgyztobe, Shar) and 2005–2006 (Barshatas, Kokpekti), the timing expected for network-wide changes of instruments or observing practice, with one later break at Bakhty (2012). Only Kainar precipitation shows a break (2009, ≈ −20%). Without metadata these cannot be confirmed as non-climatic and they are labelled candidate breaks.

Table 2. Data completeness and quality control summary.

Variable	Missing monthly values	"H"-flagged values excluded	Annual values not computed	Extreme monthly values (|z| > 5), retained	Series with candidate break
Temperature	32 of 10,800	3	5 of 900 station-years	1	6 of 15
Relative humidity	992 of 10,800 (mostly 1966–1976)	29	8 of 720 (1978–2025)	0	7 of 15
Precipitation	53 of 10,800	0	31 of 900 (3.4%)	50	1 of 15

Annual temperature and humidity require ≥ 10 months; annual precipitation requires 12 months. No observation was deleted or infilled in the main analysis.

Table 3. Candidate inhomogeneities detected by SNHT and Pettitt tests on relative series (flag: SNHT $p < 0.01$, Pettitt $p < 0.05$, years ≤ 5 apart).

Variable	Station	SNHT year	Step	Pettitt year	p (SNHT)	p (Pettitt)
Temperature	Kokpekti	2006	+0.53 °C	2006	<0.001	<0.001
Temperature	Aksuat	1989	+0.34 °C	1989	0.006	0.005
Temperature	Ayagoz	2005	+0.40 °C	2005	<0.001	<0.001
Temperature	Kainar	2014	−0.32 °C	2014	0.005	0.03
Temperature	Karaul	2009	−0.33 °C	2009	<0.001	0.002
Temperature	Urzhar	2001	−0.83 °C	1997	<0.001	<0.001
Rel. humidity	Dmitrovka	1996	−2.4 pp	1996	<0.001	<0.001
Rel. humidity	Urzhar	1997	+3.7 pp	1997	<0.001	<0.001
Rel. humidity	Zhalgyztobe	1998	+1.8 pp	1998	0.002	0.003
Rel. humidity	Shar	1998	−6.9 pp	1998	<0.001	<0.001
Rel. humidity	Barshatas	2005	+3.2 pp	2005	0.002	<0.001
Rel. humidity	Kokpekti	2006	−3.0 pp	2006	0.001	0.001
Rel. humidity	Bakhty	2012	−5.2 pp	2012	<0.001	<0.001
Precipitation	Kainar	2009	−0.23 (log ratio)	2008	0.001	0.005

Step = mean after − mean before in the difference series. Temperature series were shifted by the step before the break only as a sensitivity analysis (225 of 895 station-years, 25%); no values were removed.

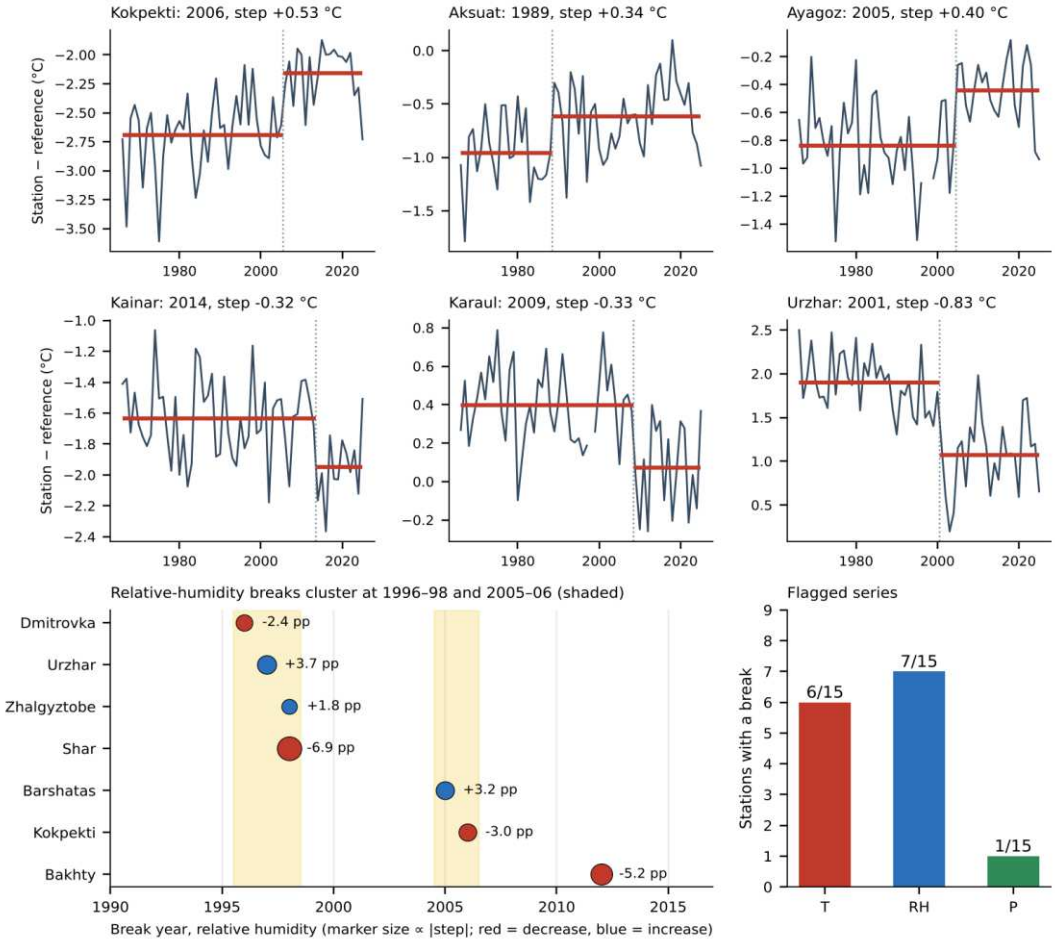

Fig. 3. Homogeneity assessment. Top: temperature difference series (station minus mean of the other 14) for the six stations with candidate breaks, with segment means (red). Bottom left: relative-humidity breaks; shaded bands mark the clusters at 1996–1998 and 2005–2006. Bottom right: number of flagged series per variable.

3.2 Spatial consistency of warming and seasonal temperature trends

Mean annual temperature of the region rose by +0.41 °C per decade (Sen slope; block-bootstrap 95% CI 0.29–0.55 °C per decade; Mann–Kendall $\tau = 0.44$, $p < 0.001$), a total of +2.4 °C over 1966–2025 (slope × 59 years; Fig. 4a; Table 4). The adjusted series gives practically the same regional rate (+0.42 °C per decade; CI 0.30–0.55). The Pettitt test locates a step change in 1989 ($p = 0.0008$): the regional mean temperature was 3.36 °C in 1966–1990 and 4.59 °C in 1991–2025, an increase of 1.2 °C. Relative to the 1991–2020 normal (4.40 °C), 2025 was the warmest year (+1.76 °C), followed by 2023 (+1.59 °C), 2007 and 2002 (+1.25 °C); the coldest were 1969 (−3.57 °C), 1984 (−2.72 °C) and 1972 (−2.18 °C). Decadal mean anomalies rose from −1.54 °C (1966–1975) through −0.65, −0.28, +0.05 and −0.04 °C to +0.74 °C in 2016–2025 (Fig. 10a).

All 15 stations warmed significantly: p (TFPW) ≤ 0.003, q ≤ 0.0026, Kendall $\tau = 0.27$–0.53. None of the 15 Sen-detrended series has significant lag-1 autocorrelation, so the TFPW procedure and the ordinary test coincide for temperature, and the Hamed–Rao variant also gives 15 of 15 significant stations. The raw station slopes range from 0.21 (Urzhar) to 0.53 °C per decade (Kokpekti), a factor of 2.5 (total change 1.2–3.1 °C), and the Urzhar slope is the only one whose 95% CI excludes the regional rate. After adjusting the six inhomogeneous series the range collapses to 0.38–0.43 °C per decade (a factor of 1.1; total change 2.3–2.5 °C) and no station differs significantly from the regional mean (Fig. 4b). The apparent contrast between "fast-warming" stations (Kokpekti, Ayagoz) and "slow-warming" stations (Urzhar, Karaul, Kainar) therefore reflects breaks in the records rather than a spatial pattern of climate change. Station warming rates are unrelated to elevation (Spearman $\rho = -0.09$, $p = 0.74$ raw; -0.19, $p = 0.50$ adjusted; Fig. 4c), latitude ($|\rho| \leq 0.05$) or longitude ($|\rho| \leq 0.35$, $p \geq 0.20$).

Table 4. Annual mean temperature trends, 1966–2025: Sen slope per decade, 95% CI, total change (slope × 59 years), TFPW Mann–Kendall p-value and FDR q-value for raw series, and slope for the series adjusted for candidate breaks (sensitivity analysis).

Station	Sen (°C/dec)	95% CI	Total ΔT (°C)	p (TFPW)	q (BH)	Adjusted Sen	Adjusted 95% CI	Break
Kainar	+0.36	0.23–0.48	+2.10	<0.001	<0.001	+0.41	0.29–0.53	2014
Aktogay	+0.41	0.29–0.55	+2.42	<0.001	<0.001	+0.41	0.29–0.55	–
Ayagoz	+0.49	0.35–0.60	+2.89	<0.001	<0.001	+0.39	0.25–0.52	2005
Barshatas	+0.39	0.27–0.51	+2.30	<0.001	<0.001	+0.39	0.27–0.51	–
Karaul	+0.35	0.21–0.52	+2.09	<0.001	<0.001	+0.42	0.28–0.56	2009
Aksuat	+0.48	0.35–0.62	+2.83	<0.001	<0.001	+0.40	0.27–0.54	1989
Kokpekti	+0.53	0.39–0.67	+3.10	<0.001	<0.001	+0.43	0.25–0.55	2006
Urzhar	+0.21	0.07–0.32	+1.23	0.003	0.0026	+0.41	0.29–0.51	2001
Zhalgyztobe	+0.41	0.25–0.55	+2.41	<0.001	<0.001	+0.41	0.25–0.55	–
Bakhty	+0.42	0.29–0.53	+2.45	<0.001	<0.001	+0.42	0.29–0.53	–
Dmitrovka	+0.42	0.27–0.59	+2.49	<0.001	<0.001	+0.42	0.27–0.59	–
Shalabay	+0.38	0.23–0.55	+2.25	<0.001	<0.001	+0.38	0.23–0.55	–
Shar	+0.41	0.24–0.55	+2.42	<0.001	<0.001	+0.41	0.24–0.55	–
Semey	+0.42	0.26–0.59	+2.46	<0.001	<0.001	+0.42	0.26–0.59	–
Semyarka	+0.41	0.23–0.58	+2.40	<0.001	<0.001	+0.41	0.23–0.58	–
Region (mean of 15)	**+0.41**	**0.29–0.55**	**+2.43**	**<0.001**	–	**+0.42**	**0.30–0.55**	**1989 (step)**

Stations ordered by elevation (high to low). Regional CI is a block-bootstrap interval. The regional adjusted slope is that of the mean of adjusted station series.

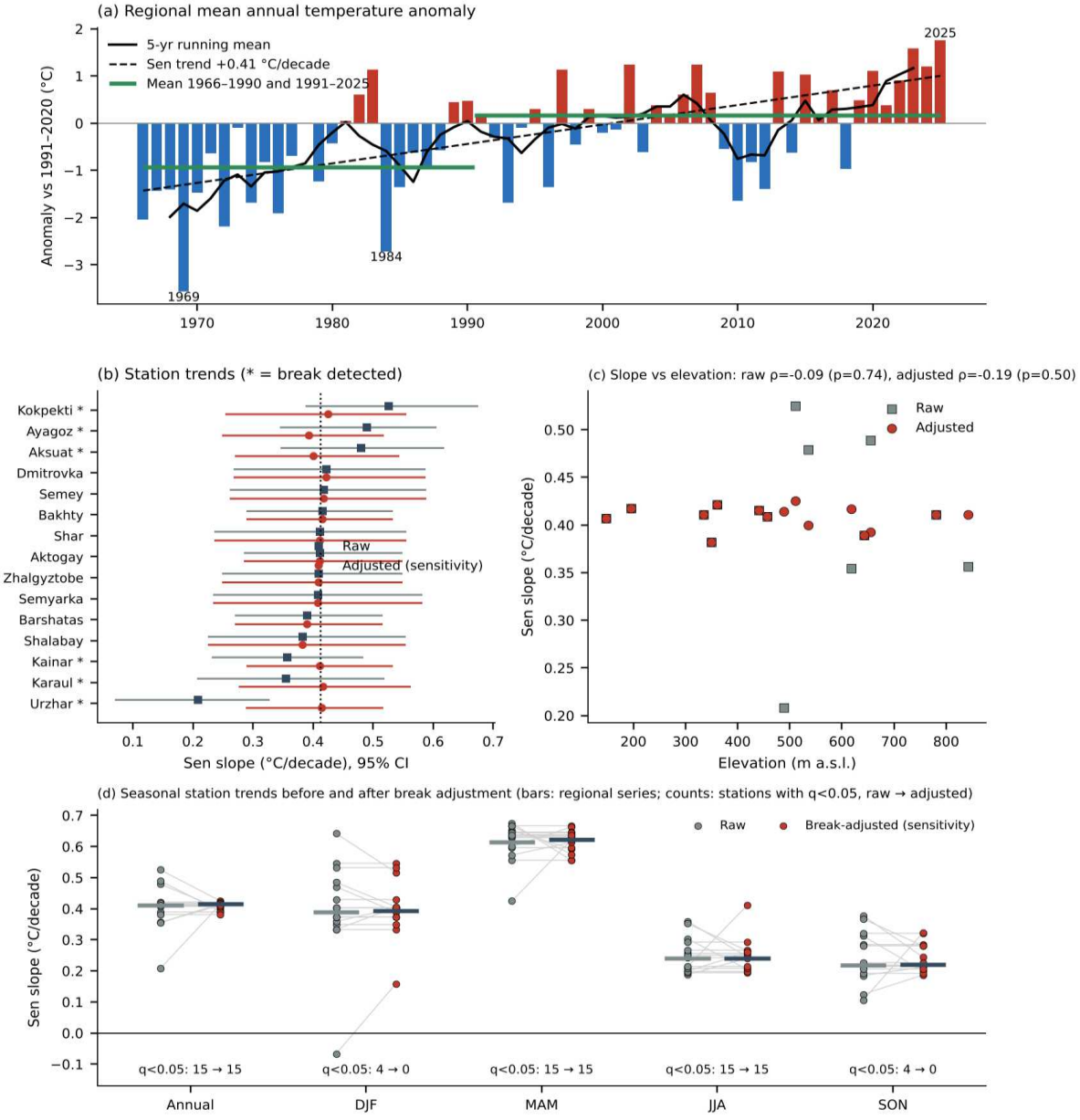

Fig. 4. Temperature change. (a) Regional mean annual temperature anomaly relative to 1991–2020 with 5-year running mean, Sen trend and the means before and after the 1989 break. (b) Station Sen slopes with 95% CI for raw (grey) and break-adjusted (red)

series; stars mark stations with a detected break. (c) Station slope versus elevation. (d) Station Sen slopes of seasonal temperature from raw and break-adjusted series (numbers of stations with $q < 0.05$: raw → adjusted).

Warming is strongly seasonal (Table 5, Figs. 5 and 6). Spring (MAM) warms fastest at +0.61 °C per decade (+3.6 °C over 1967–2025; $p < 0.001$) and is significant at all 15 stations, followed by winter (+0.39 °C per decade; $p = 0.05$), summer (+0.24 °C per decade; $p < 0.001$; all 15 stations) and autumn (+0.22 °C per decade; $p = 0.03$). Winter and autumn series are noisy, so only 4 stations remain significant after FDR control in each, and these station-level results are not robust: after adjusting the six inhomogeneous records no station is significant in winter or autumn, whereas regional rates are unchanged (+0.39 and +0.22 °C per decade). Spring (+0.62 °C per decade, 15 of 15 stations) and summer (+0.24) are robust to the adjustment (Table 5, Fig. 4d). The spring rate is 2.5 times the summer rate.

Seasonal precipitation trends are small and statistically indistinguishable from zero in every season at the regional scale ($|\Delta| \leq 2.2$ mm per decade; $p = 0.23$–0.40), although their signs are consistent: spring precipitation declines at 13 of 15 stations (−1.59 mm per decade, $p = 0.29$; only Kainar significant after FDR, and Kainar has a precipitation break in 2009), while summer precipitation increases at 14 of 15 (+2.20 mm per decade, $p = 0.27$). Relative humidity falls in spring (−0.78 percentage points per decade, $p = 0.015$; negative at 10 of 15 stations, $q < 0.05$ at 5) but not in other seasons (DJF +0.12, JJA −0.09, SON +0.51 pp per decade, all $p > 0.1$). The only season in which temperature rises fast, humidity falls and precipitation tends to decline is therefore spring.

Table 5. Trends of regional mean annual and seasonal series (mean of 15 stations) and station-level summary.

Variable	Season	n (years)	Sen slope per decade	Total change	p (TFPW)	Stations q < 0.05	Stations (+ / −)	Adj. Sen per decade	Adj. stations q < 0.05
Temperature	Annual	60	+0.41 °C	+2.4 °C	<0.001	15	15 / 0	+0.42 °C	15
	DJF	59	+0.39 °C	+2.3 °C	0.05	4	14 / 1	+0.39 °C	0
	MAM	60	+0.61 °C	+3.6 °C	<0.001	15	15 / 0	+0.62 °C	15
	JJA	60	+0.24 °C	+1.4 °C	<0.001	15	15 / 0	+0.24 °C	15
	SON	60	+0.22 °C	+1.3 °C	0.03	4	15 / 0	+0.22 °C	0
Relative humidity (1978–2025)	Annual	48	−0.01 pp	−0.1 pp	0.94	4	9 / 6	–	–
	DJF	47	+0.12 pp	+0.6 pp	0.47	0	9 / 6	–	–
	MAM	48	−0.78 pp	−3.7 pp	0.02	5	4 / 10	–	–
	JJA	48	−0.09 pp	−0.4 pp	0.68	2	9 / 4	–	–
	SON	48	+0.51 pp	+2.4 pp	0.14	5	11 / 3	–	–
Precipitation	Annual	58	+1.34 mm	+7.9 mm	0.66	0	11 / 4	–	–
	DJF	59	+1.52 mm	+8.8 mm	0.23	0	12 / 3	–	–
	MAM	60	−1.59 mm	−9.4 mm	0.29	1	2 / 13	–	–
	JJA	60	+2.20 mm	+13.0 mm	0.27	0	14 / 1	–	–
	SON	60	+1.45 mm	+8.6 mm	0.40	0	12 / 3	–	–

Relative humidity and precipitation are regional means of station anomalies. Counts refer to the 15 station series (raw). Total change = Sen slope × (last year − first year of the series). Adj. = temperature series shifted for the six candidate breaks (sensitivity analysis, Section 2.2). The Sen slope sign convention is positive = increase.

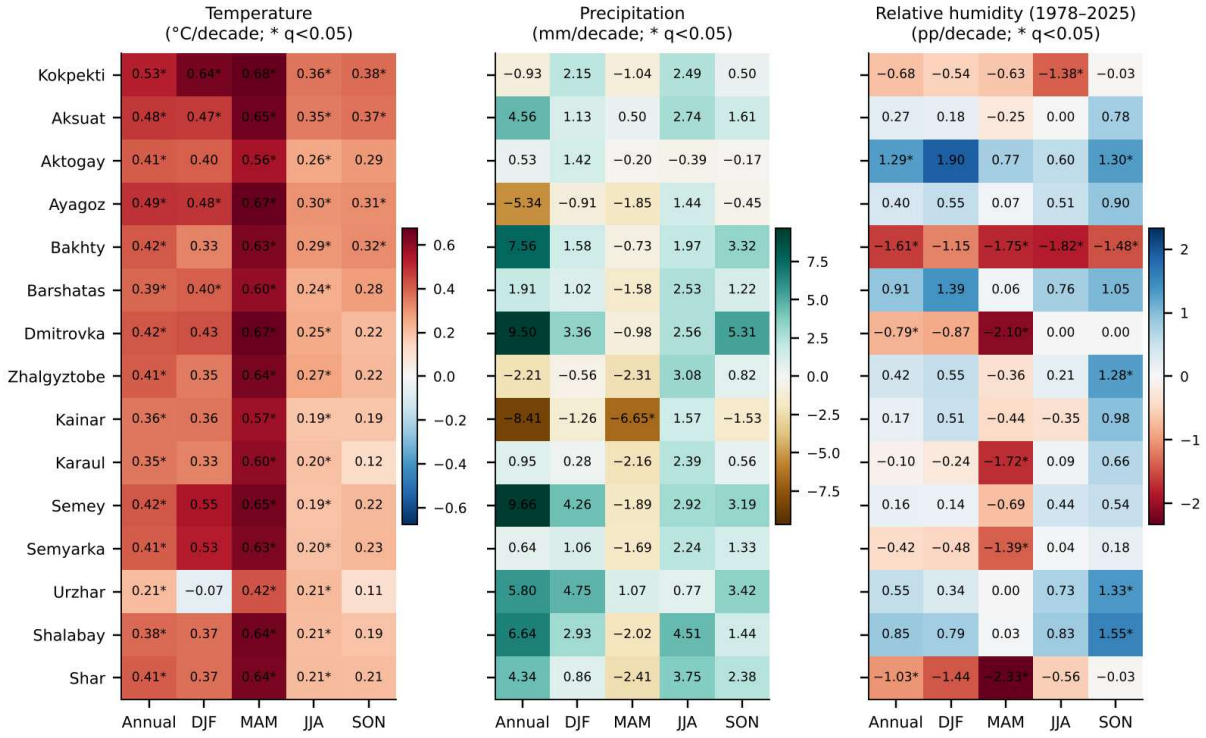

Fig. 5. Station-by-season trends (Sen slope per decade) of temperature, precipitation and relative humidity; asterisks mark BH-FDR q < 0.05. Stations ordered as in Table 1 (north-west to south-east not implied).

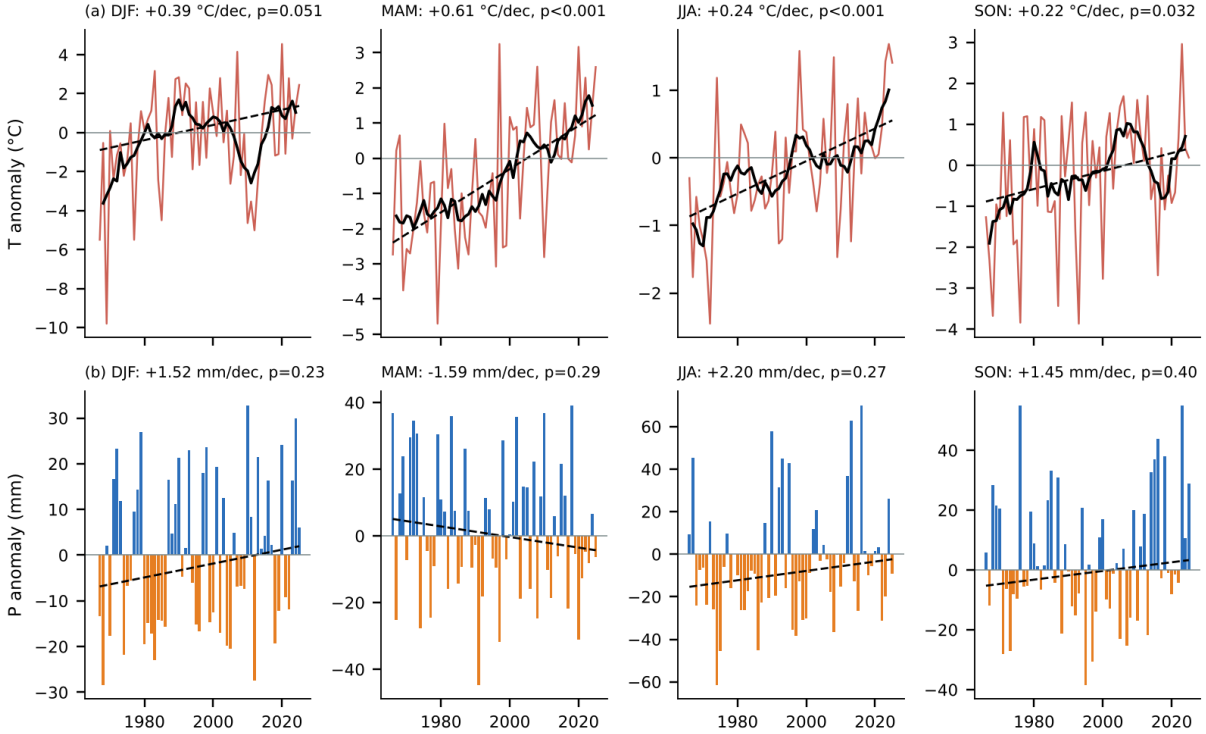

Fig. 6. Regional seasonal anomalies (relative to 1991–2020). (a) Seasonal temperature (thin line), 7-year mean (black) and Sen trend (dashed). (b) Seasonal precipitation anomalies (bars) and Sen trend.

Station values of trend magnitude are mapped in Fig. 7 without interpolation. Annual and spring warming are spatially uniform once the records are adjusted for breaks, and the only structure in the precipitation, humidity and SPEI trends is that of noise: sign changes occur between neighbouring stations (e.g., Kainar and Aktogay, 100–250 km apart) and the few significant humidity trends coincide with stations that have breaks (Section 3.3). Station trends of temperature, precipitation, humidity and SPEI-6 show no robust association with elevation, latitude or longitude (all $q \geq 0.24$; Section 3.7), and cross-validation shows that no spatial predictor, including regression kriging, predicts trend magnitudes better than the regional mean (Table 13). The sign-based classification of stations into "warming–wetting", "warming–drying" and "mixed" regimes that is common in the literature is therefore not statistically supported: 14 of 15 station precipitation

trends and 11 of 15 humidity trends are not significant, so a classification by the sign of non-significant slopes would map sampling noise.

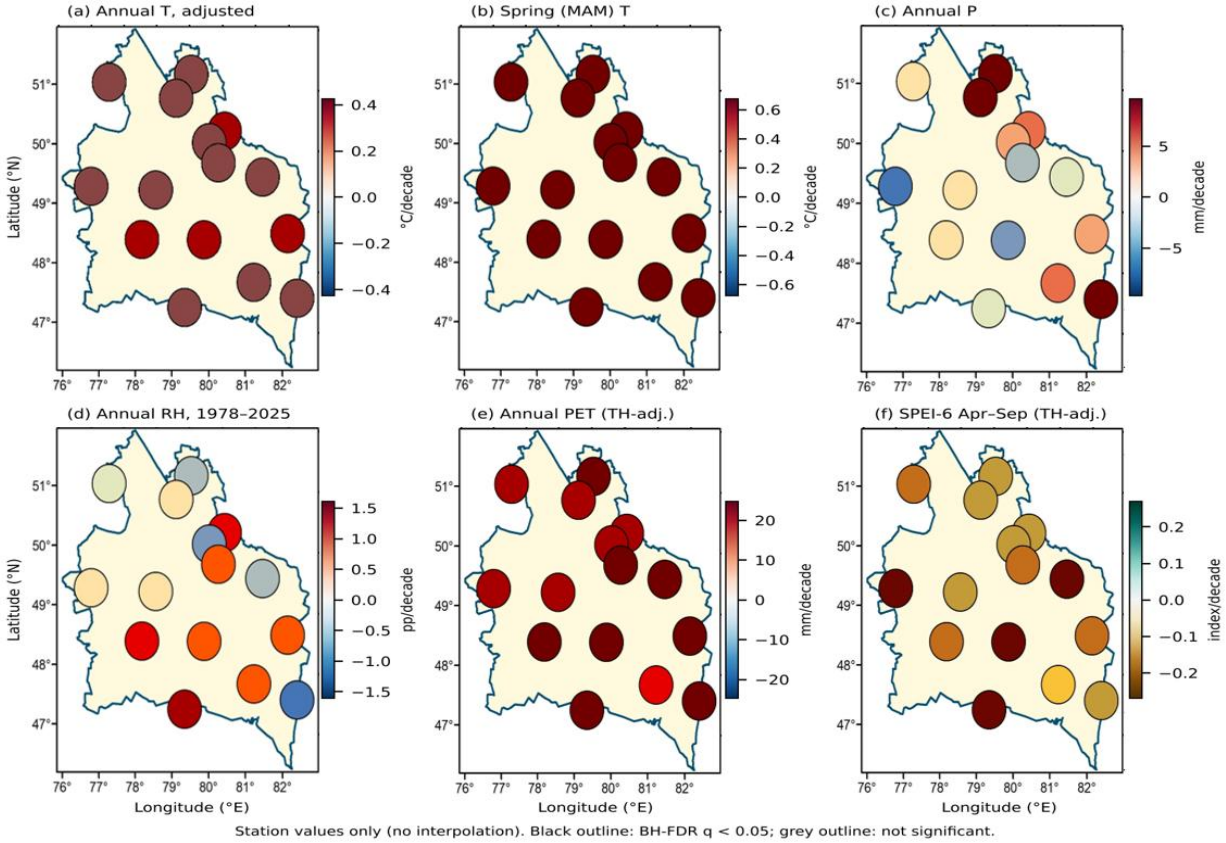

Fig. 7. Station values of trend magnitudes, 1966–2025 (humidity 1978–2025): (a) annual temperature (break-adjusted), (b) spring temperature, (c) annual precipitation, (d) annual relative humidity, (e) annual PET (TH-adj.) and (f) SPEI-6 for April–September (TH-adj.). Marker size is proportional to |trend|; black outlines mark BH-FDR q < 0.05. No interpolation is applied.

3.3 Trends and variability of relative humidity and precipitation

The regional annual relative humidity trend is zero (−0.01 percentage points per decade, p = 0.94; Table 5). Four stations have significant annual trends after FDR control (Table 6, Fig. 8a): Aktogay increases (+1.29 pp per decade, q = 0.001) while Bakhty (−1.61), Shar (−1.03) and Dmitrovka (−0.79 pp per decade) decrease. Three of the four significant stations have candidate breaks (Bakhty 2012, Shar 1998, Dmitrovka 1996) and the magnitude of their trends is comparable to the break steps (−5.2, −6.9 and −2.4 pp), so these trends cannot be separated from instrument changes; Aktogay's series has a borderline shift (SNHT p = 0.028; Pettitt p = 0.012, 2014) that did not meet the flagging rule. Residual autocorrelation is significant at 9 of 15 stations, which is why the pre-whitened test is used; with the Hamed–Rao variant the number of significant stations would rise to 9, an inflation we judge spurious. Regional humidity anomalies (Fig. 8b) are dominated by interannual variability, with record-dry years in 1997 (−5.2 pp) and 2008 (−3.9 pp) and the wettest in 2016 (+4.9 pp). The spring decline (−0.78 pp per decade; Fig. 8c) is the one humidity signal that is regionally coherent, and it persists at two stations without detected breaks (Karaul, Semyarka) in addition to Bakhty, Shar and Dmitrovka.

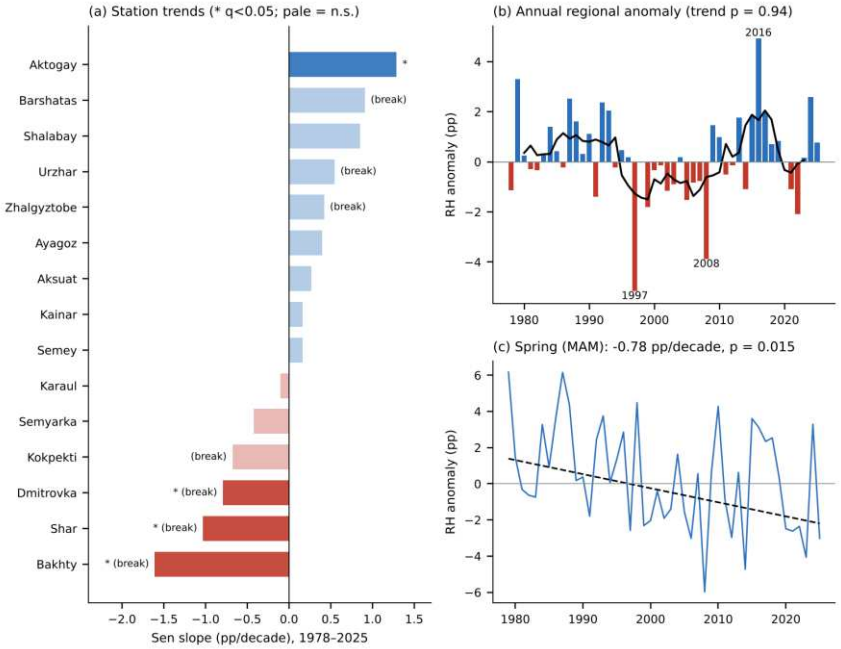

Fig. 8. Relative humidity, 1978–2025. (a) Annual Sen slopes by station; "(break)" marks stations with a detected inhomogeneity and asterisks q < 0.05. (b) Regional annual anomaly relative to 1991–2020. (c) Regional spring (MAM) anomaly with Sen trend.

Regional annual precipitation shows no trend (+1.34 mm per decade, a total of +7.9 mm or about +2.8% of the normal over 1966–2025; p = 0.66; Fig. 9b). Station slopes range from −8.4 to +9.7 mm per decade, 11 of 15 are positive, and only Kainar is significant before FDR control (−8.4 mm per decade, p = 0.026, q = 0.34); the Kainar decline coincides with its 2009 break and is not robust (Table 6, Fig. 9a). No seasonal precipitation trend is significant at the regional scale (Table 5). The region is characterised by very large year-to-year swings: the driest years were 1974 (−122 mm, −43% of the normal), 2008 (−35%), 1991 (−31%) and 1997 (−30%), the wettest 2016 (+128 mm, +45%), 1966 (+30%), 2024 and 1990. Decadal means of the regional anomaly alternate between −6.4% (1996–2005) and +6.0% (2016–2025).

Table 6. Annual relative-humidity (1978–2025) and precipitation (1966–2025) trends by station.

Station	RH Sen (pp/dec)	p (TFPW)	q (BH)	AR sig.	RH break	P Sen (mm/dec)	P Sen (% normal/dec)	p (TFPW)	q (BH)	P break
Kainar	+0.17	0.90	0.898	Y	–	−8.4	−3.6	0.03	0.34	2009
Aktogay	+1.29	<0.001	<0.001	Y	–	+0.5	+0.3	0.93	0.93	–
Ayagoz	+0.40	0.15	0.205	n	–	−5.3	−1.9	0.40	0.71	–
Barshatas	+0.91	0.02	0.063	Y	2005	+1.9	+0.9	0.69	0.93	–
Karaul	−0.10	0.54	0.583	Y	–	+1.0	+0.4	0.82	0.93	–
Aksuat	+0.27	0.43	0.497	Y	–	+4.6	+2.1	0.30	0.71	–
Kokpekti	−0.68	0.03	0.063	n	2006	−0.9	−0.3	0.90	0.93	–
Urzhar	+0.55	0.12	0.185	Y	1997	+5.8	+1.3	0.42	0.71	–
Zhalgyztobe	+0.42	0.10	0.173	n	1998	−2.2	−0.7	0.58	0.87	–
Bakhty	−1.61	<0.001	<0.001	n	2012	+7.6	+2.5	0.26	0.71	–
Dmitrovka	−0.79	<0.001	0.002	n	1996	+9.5	+2.9	0.07	0.34	–
Shalabay	+0.85	0.03	0.063	Y	–	+6.6	+2.0	0.20	0.71	–
Shar	−1.03	0.007	0.025	Y	1998	+4.3	+1.5	0.38	0.71	–
Semey	+0.16	0.33	0.414	Y	–	+9.7	+3.2	0.06	0.34	–
Semyarka	−0.42	0.08	0.144	n	–	+0.6	+0.3	0.87	0.93	–
Region	**−0.01**	**0.94**	**–**	**–**	**–**	**+1.3**	**+0.5**	**0.66**	**–**	**–**

AR sig. = significant lag-1 autocorrelation of detrended series (Y/n). Percent of normal uses the 1991–2020 annual precipitation normal of each station.

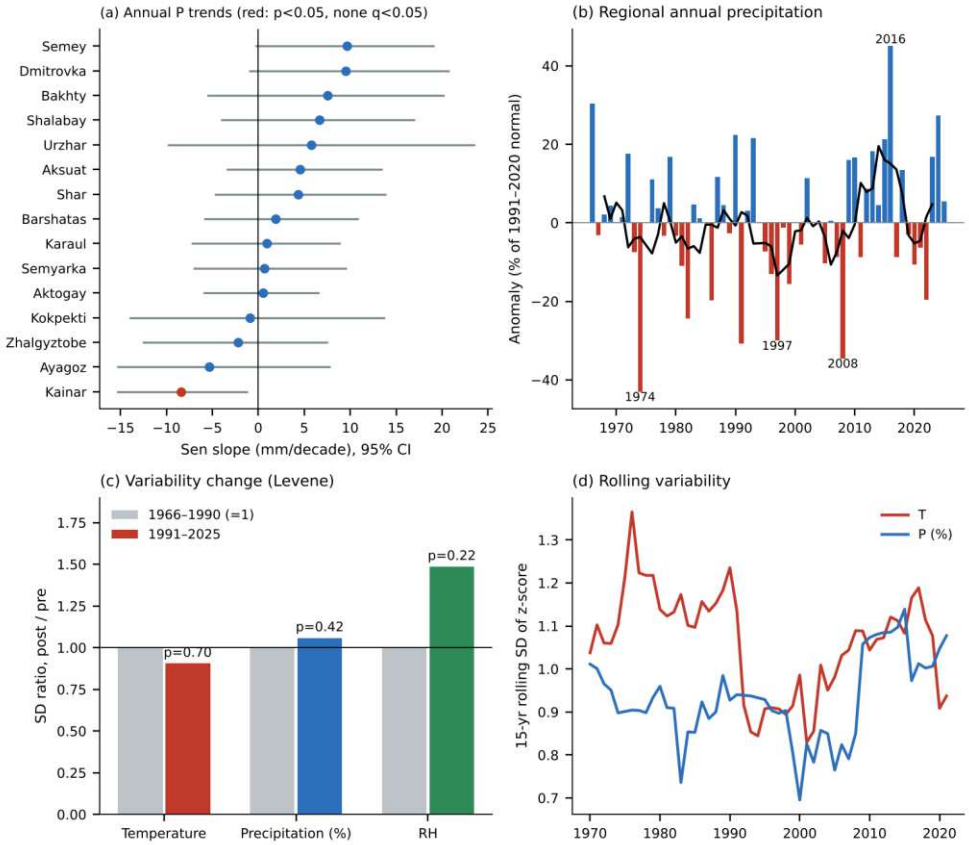

Fig. 9. Precipitation. (a) Annual Sen slopes with 95% CI (red: $p < 0.05$ before FDR). (b) Regional annual anomaly as percent of the 1991–2020 normal with 5-year mean. (c) Ratio of the standard deviation of regional anomalies 1991–2025 to 1966–1990 with Levene p-values. (d) 15-year rolling standard deviation of standardized anomalies.

3.4 Climate normal and variability of anomalies

The regional 1991–2020 normals are 4.40 °C for temperature, 281 mm for annual precipitation and 63.5% for relative humidity (Table 7). Using the full-record mean instead of the WMO normal would shift temperature anomalies by 0.29 °C (4.40 vs 4.11 °C) without changing any trend, but would understate recent deviations. The mean temperature anomaly changed from −0.92 °C in 1966–1990 to +0.17 °C in 1991–2025 (difference +1.09 °C, Welch $p = 0.0002$). The frequency of warm years ($z \geq +1$) rose from 1 of 25 years (4%) to 10 of 35 (29%), whereas the frequency of cold years ($z \leq -1$) fell from 12 of 25 (48%) to 5 of 35 (14%) (Fig. 10).

Claims of an “increasing amplitude” of precipitation anomalies are not supported by the homogeneous record. The standard deviation of regional precipitation anomalies changed from 15.3% (1966–1990) to 17.1% (1991–2025) of the normal, a ratio of 1.06 that is not significant (Levene $p = 0.42$); the Sen trend of the absolute standardized anomaly is also insignificant ($p = 0.16$), no station has a significantly larger variance after 1991 ($q \geq 0.05$ for all 15 stations), and the frequencies of wet ($z \geq +1$: 12% vs 14%) and dry years ($z \leq -1$: 12% vs 11%) are unchanged (Fig. 9c,d; Fig. 10). Temperature variability decreased slightly (SD 1.10 → 0.93 °C, $p = 0.70$), so the shift to a “new thermal normal” is a displacement of the mean, not a change of amplitude. For humidity the post-1991 SD is larger (1.24 → 1.85 pp, $p = 0.22$), but the pre-1991 sample has only 13 years and the series contain breaks. We therefore describe precipitation as highly but stably variable.

Table 7. Climatological normals 1991–2020 (T, P, RH) and mean annual PET and aridity index P/PET (1966–2025) by station.

Station	T (°C)	P (mm)	RH (%)	PET TH (mm)	PET TH-adj. (mm)	P/PET (TH)	P/PET (TH-adj.)	Class (TH-adj.)
Kainar	2.8	232	63.2	543	641	0.43	0.37	semi-arid
Aktogay	7.0	196	56.8	685	898	0.28	0.21	semi-arid
Ayagoz	3.8	287	64.3	586	779	0.53	0.40	semi-arid
Barshatas	4.5	217	60.2	604	857	0.35	0.25	semi-arid
Karaul	4.7	234	57.9	594	732	0.41	0.33	semi-arid
Aksuat	3.8	214	63.2	616	810	0.33	0.25	semi-arid
Kokpekti	2.2	296	64.8	573	702	0.55	0.45	semi-arid
Urzhar	5.6	453	65.9	641	736	0.71	0.62	dry sub-humid
Zhalgyztobe	4.4	303	62.6	606	779	0.50	0.39	semi-arid
Bakhty	7.0	306	64.0	663	804	0.45	0.37	semi-arid
Dmitrovka	3.5	331	67.2	582	701	0.58	0.48	semi-arid
Shalabay	4.3	332	67.3	597	731	0.56	0.46	semi-arid
Shar	3.8	291	65.4	596	771	0.49	0.38	semi-arid
Semey	4.4	301	65.7	613	723	0.47	0.40	semi-arid
Semyarka	4.2	220	64.1	627	846	0.35	0.26	semi-arid
Region	**4.4**	**281**	**63.5**	**608**	**767**	**0.47**	**0.37**	**semi-arid**

PET TH-adj. = Thornthwaite PET adjusted to the Penman–Monteith level (Section 2.4). UNEP classes: 0.2–0.5 semi-arid, 0.5–0.65 dry sub-humid. P/PET with Thornthwaite PET classifies 9 stations as semi-arid, 5 dry sub-humid and Urzhar (0.71) as humid. The regional row is the mean of the 15 station values.

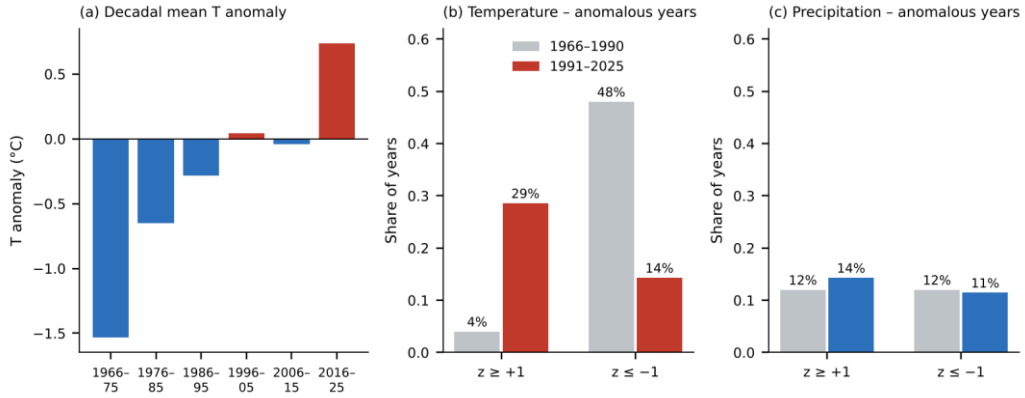

Fig. 10. Anomalies relative to 1991–2020. (a) Decadal mean temperature anomaly of the regional mean. (b, c) Share of years with standardized anomaly $z \geq +1$ and $z \leq -1$ before and after 1991 for temperature (b) and precipitation (c); z is standardized by the 1991–2020 standard deviation.

3.5 Evaporative demand, climatic water balance and drought dynamics

Over the 2001–2024 overlap the three PET formulations differ strongly in level (Fig. 11a). Mean annual PET is 627 mm for Thornthwaite, 921 mm for Hargreaves–Samani and 861 mm for Penman–Monteith; Thornthwaite is therefore 27% below the FAO-56 reference (station ratios PM/TH of 1.23–1.54), whereas Hargreaves–Samani overestimates it by 7% on average (0.94–1.30). Thornthwaite is weakest in the shoulder months, when its temperature-only formulation underestimates the radiative and aerodynamic terms: the calibration factor PM/TH is 1.5–2.1 in April and 1.5–2.3 in October but 1.0–1.2 in July (Fig. 11c; the factor is set to 1 where mean monthly Thornthwaite PET is below 10 mm, which concerns only March at Bakhty). Agreement in monthly values including the seasonal cycle is high ($r = 0.97$–0.99 between all pairs), but agreement in interannual variability is moderate: the within-station correlation of annual totals is 0.53 on average for TH–PM (0.19–0.79), 0.72 for HS–PM (0.52–0.93) and 0.79 for TH–HS. Thornthwaite therefore captures the level of temperature-driven demand only partially and none of the humidity or wind influence, which is why trend conclusions are reported for both the Thornthwaite and the TH-adj. series.

Trends over the same 24 years differ between methods (regional means of station anomalies): Thornthwaite +19.1 mm per decade (95% CI 0.1 to 36.7; $p = 0.045$), Hargreaves–Samani +17.0 (5.0 to 35.9; $p = 0.024$) and Penman–Monteith +8.1 mm per decade (−14.2 to +31.0; $p = 0.46$; 22 years with at least 12 stations), with positive slopes at 15, 13 and 8 of 15 stations, respectively. A 24-year window is too short for precise trends and the intervals overlap, but the comparison shows that the magnitude of the temperature-based PET increase is uncertain and probably an upper estimate (the Penman–Monteith trend is less than half of the Thornthwaite trend and not significant), because Penman–Monteith also responds to humidity, radiation and wind.

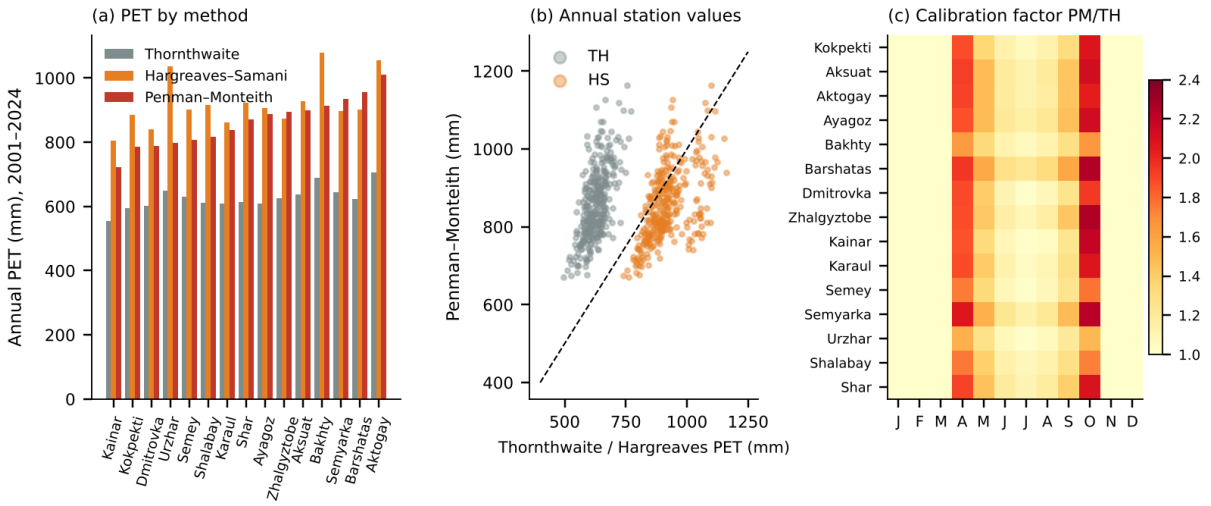

Fig. 11. Evaporative demand by method, 2001–2024. (a) Mean annual PET by station. (b) Annual station values of Thornthwaite and Hargreaves–Samani PET against Penman–Monteith (dashed: 1:1). (c) Calibration factors PM/TH by station and month (factor 1 where mean TH < 10 mm).

The long-term aridity index confirms a semi-arid climate (Table 7): P/PET averages 0.47 with Thornthwaite and 0.37 with TH-adj. PET (station ranges 0.28–0.71 and 0.21–0.62), and with TH-adj. PET 14 of 15 stations are semi-arid; only Urzhar, at the foot of the Tarbagatai (mean precipitation 454 mm), is dry sub-humid. The water balance is negative everywhere: regional P − PET averages −326 mm (TH) and −485 mm (TH-adj.) per year.

Evaporative demand has risen at every station (Table 8, Fig. 12): regional PET (mean of station anomalies) increases by +13.3 mm per decade (Thornthwaite) or +19.4 mm per decade (TH-adj.), about 2–3% per decade ($p < 0.001$; $q < 0.05$ at 15 of 15 stations), compared with a precipitation change of +1.3 mm per decade ($p = 0.66$), which offsets only 7–10% of the rise. As a result, the annual climatic water balance P − PET declines by −10.4 mm per decade with Thornthwaite ($p = 0.032$; negative at all 15 stations, $q < 0.05$ at 2) and by −16.7 mm per decade with TH-adj. PET ($p = 0.007$; $q < 0.05$ at 9 stations). The aridity index itself shows no significant trend (−0.007 per decade, $p = 0.24$–0.28, one station significant), because the index is a ratio dominated by the much larger PET and a change of −0.007 corresponds to only 1.5–2% of its mean per decade. Interannual variability of the balance, in contrast, is controlled by precipitation: P explains on average 57% (44–72%) of the variance of detrended P − PET ($r = +0.94$), versus a PET correlation of −0.74, and wet years have lower PET ($r(P, PET) = −0.47$) so the two terms reinforce each other (Fig. 18d). Precipitation sets the year-to-year drought severity; temperature-driven PET sets its drift.

Table 8. Regional mean and trend of the annual water balance components, 1966–2025.

Variable	Mean	Sen slope per decade	p (TFPW)	Stations q < 0.05 (of 15)
Precipitation, P (mm)	283	+1.34	0.66	0
PET, Thornthwaite (mm)	608	+13.3	<0.001	15
PET, TH-adj. (mm)	767	+19.4	<0.001	15
P − PET, Thornthwaite (mm)	−326	−10.4	0.03	2
P − PET, TH-adj. (mm)	−485	−16.7	0.007	9
P/PET, Thornthwaite	0.47	−0.007	0.28	1
P/PET, TH-adj.	0.38	−0.007	0.24	1

Regional values are means of station anomalies added to the network-mean climatology (≥ 12 stations per year; 58–60 years), so means can differ in the last digit from the station averages in Table 7. Station counts use BH-FDR within each variable.

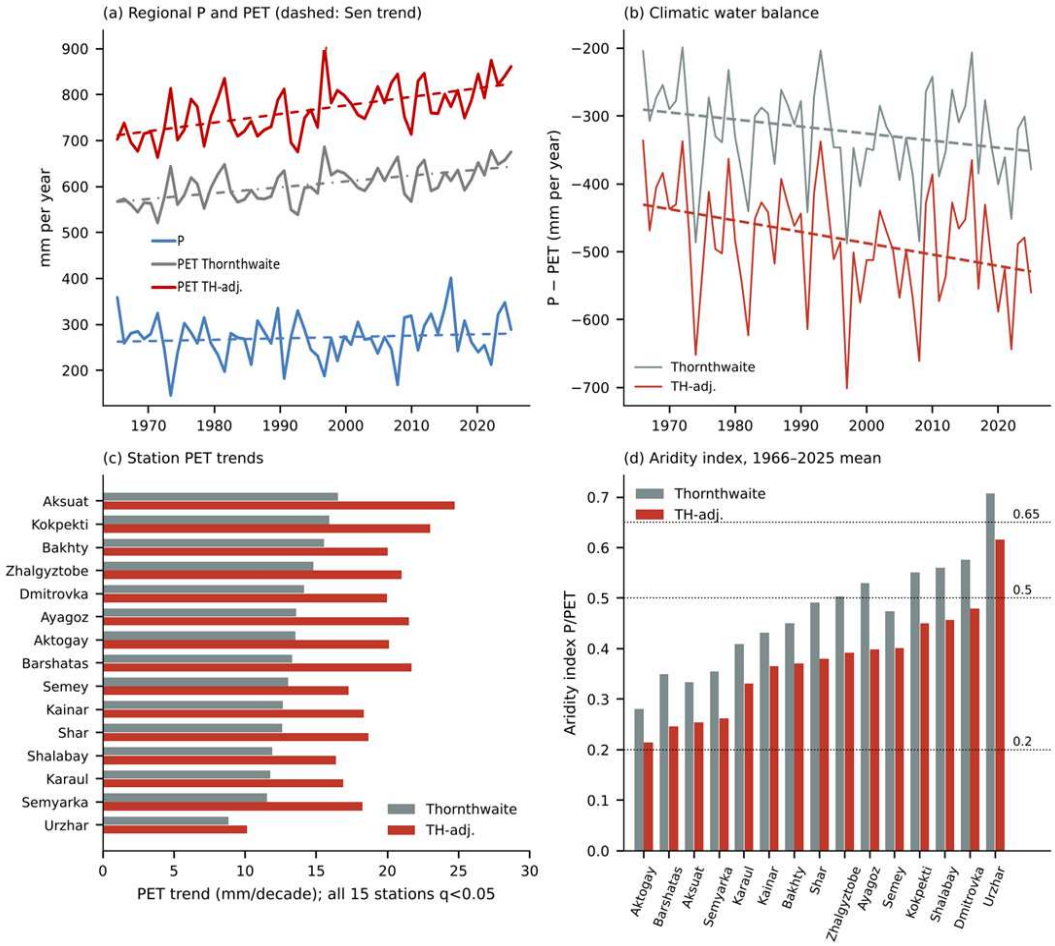

Fig. 12. Water balance. (a) Regional mean annual precipitation and PET (Thornthwaite, TH-adj.) with Sen trends (dashed); regional means of station anomalies. (b) Climatic water balance P - PET. (c) Station PET trends for both PET series (all q < 0.05). (d) Aridity index P/PET by station with UNEP class boundaries.

Precipitation-only SPI shows no trend at any time scale (Table 9): the regional annual SPI-12 changes by +0.04 per decade (p = 0.53), SPI-6 for April–September by +0.01 (p = 0.87), and SPI-3 for spring by −0.04 (p = 0.49). The SPEI, which includes evaporative demand, declines instead (Figs. 13a and 14). The decline is concentrated in spring and the growing season: SPEI-3 for March–May changes by −0.18 per decade with Thornthwaite PET (p = 0.021) and −0.21 with TH-adj. PET (p = 0.004), and SPEI-6 for April–September by −0.18 (p = 0.006) and −0.21 per decade (p = 0.002). SPEI-6 declines at all 15 stations with either PET series; it is significant after FDR control at 3 stations with Thornthwaite PET and at 14 stations with TH-adj. PET (Fig. 13b, Fig. 7f). Annual SPEI-12 is marginal with Thornthwaite PET (−0.12 per decade, p = 0.060; 1 station significant) and significant with TH-adj. PET (−0.16 per decade, p = 0.01; 5 stations). Winter, summer and autumn trends are not significant for any PET choice (summer −0.07 to −0.08 per decade, p = 0.09–0.15). Because SPI does not change while SPEI does, the drying is attributable to evaporative demand, consistent with the warming and spring humidity decline reported above; the two PET versions share the temperature-driven variability and differ mainly in level, so they are not independent estimates; the conclusions that hold for both (the sign, the seasonality, and the SPI–SPEI contrast) are the robust ones, whereas the number of stations with significant drying depends on the PET choice.

Table 9. Trends of regional mean SPEI and SPI (index units per decade), 1967–2025.

Index	Time scale / season	Sen slope per decade	p (TFPW)	Stations significantly drier (q < 0.05)	Stations with negative slope
SPEI, Thornthwaite	Annual (12-month)	−0.117	0.06	1	15
	DJF (3-month)	+0.082	0.22	0	3
	MAM (3-month)	−0.176	0.02	1	15
	JJA (3-month)	−0.072	0.15	0	15
	SON (3-month)	−0.022	0.73	0	10
	Apr–Sep (6-month)	−0.178	0.006	3	15
SPEI, TH-adj.	Annual (12-month)	−0.158	0.01	5	15
	DJF (3-month)	+0.082	0.22	0	3
	MAM (3-month)	−0.206	0.004	14	15
	JJA (3-month)	−0.084	0.09	0	15
	SON (3-month)	−0.048	0.46	0	10
	Apr–Sep (6-month)	−0.206	0.002	14	15
SPI	Annual (12-month)	+0.038	0.53	0	3
	DJF (3-month)	+0.080	0.24	0	3
	MAM (3-month)	−0.038	0.49	1	12
	JJA (3-month)	+0.069	0.17	0	0
	SON (3-month)	+0.055	0.37	0	3
	Apr–Sep (6-month)	+0.012	0.86	0	4

SPEI/SPI for a season use accumulation ending in the last month of the season (see Section 2.4). The regional series is the mean of ≥ 12 stations. Shaded rows highlight the significant spring and growing-season signals.

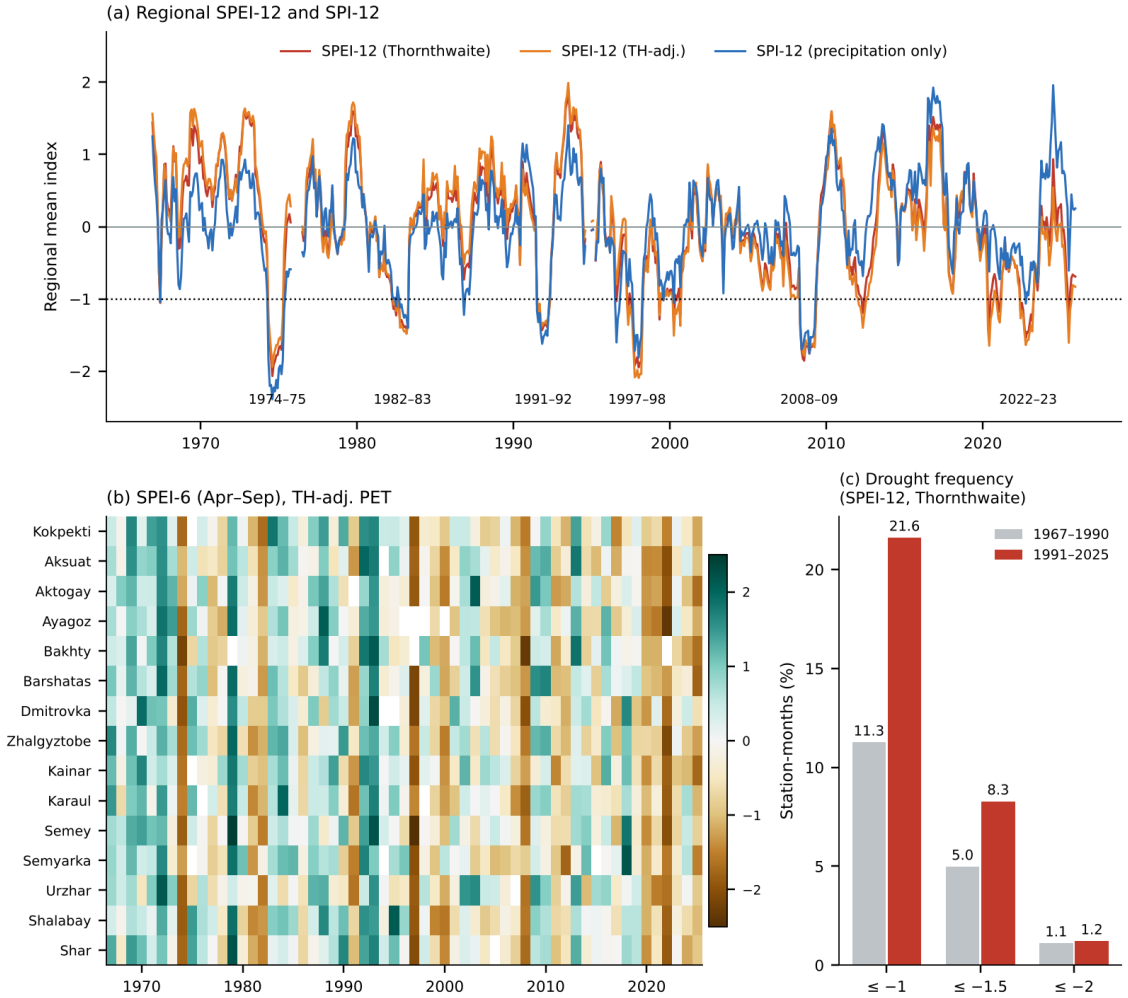

Fig. 13. Droughts, 1966–2025. (a) Regional mean SPEI-12 (Thornthwaite and TH-adj. PET) and precipitation-only SPI-12; years label the largest events. (b) Station SPEI-6 for April–September (TH-adj.) by year. (c) Share of station-months below SPEI-12 thresholds in 1967–1990 and 1991–2025.

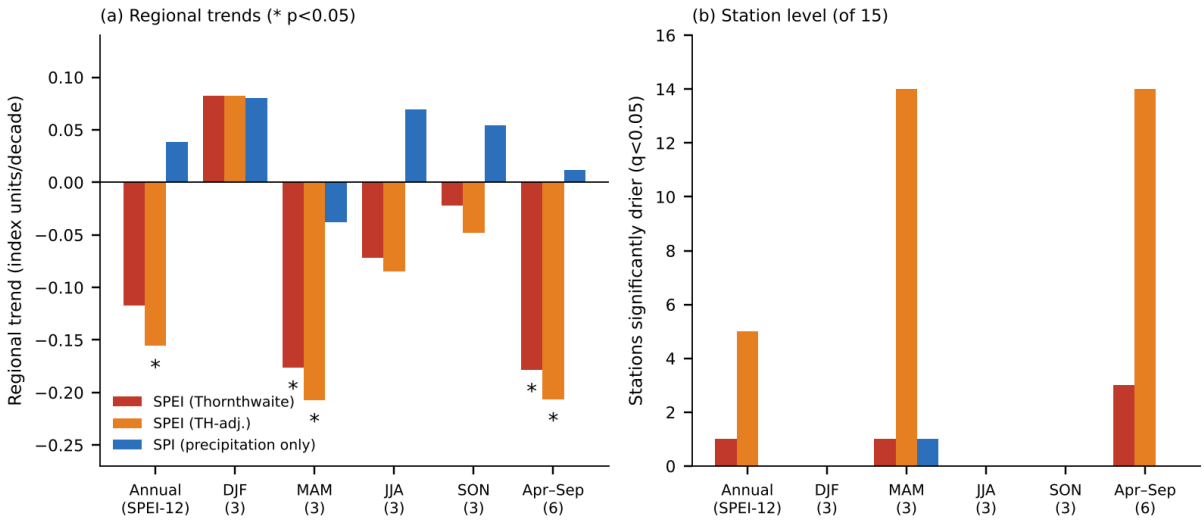

Fig. 14. Trends of drought indices. (a) Regional trend by season/time scale for SPEI (Thornthwaite and TH-adj.) and SPI; asterisks mark $p < 0.05$. (b) Number of stations (of 15) with a significant drying trend after FDR control.

Table 10. Regional drought events (regional mean SPEI-12 ≤ −1 for ≥ 3 months, Thornthwaite PET).

Start	End	Duration (months)	Severity (Σ|SPEI|)	Peak SPEI-12
1974-05	1975-04	12	20.7	−2.07
1982-04	1982-07	4	4.5	−1.23
1982-09	1983-04	8	10.6	−1.42
1991-07	1992-05	11	14.0	−1.43
1997-07	1998-04	10	16.2	−1.95
2008-05	2009-05	13	21.3	−1.85
2022-06	2023-03	10	13.1	−1.54

The share of station-months with SPEI-12 ≤ −1 rose from 11.3% (1967–1990) to 21.6% (1991–2025), a ratio of 1.9; for ≤ −1.5 from 5.0% to 8.3% (1.7); for ≤ −2 from 1.1% to 1.2% (1.1).

Seven drought episodes reach the regional criterion (Table 10): three in 1967–1990 and four in 1991–2025. The longest and most severe are 1974–75 (12 months, peak −2.07), 2008–09 (13 months, peak −1.85) and 1997–98 (peak −1.95), followed by 2022–23 (peak −1.54), 1991–92 and the two phases of 1982–83. The 2008–09 and 1974–75 events were of almost equal severity; the former coincides with one of the driest humidity years (2008) and the latter with the driest precipitation year of the record (1974). The number of regional episodes therefore rose only from three to four over a longer period, but the share of station-months in moderate and severe drought nearly doubled (×1.9 and ×1.7), i.e. droughts became spatially more extensive; extreme drought (SPEI-12 ≤ −2) did not become more common, in line with the unchanged precipitation variability (Section 3.4).

3.6 Relationships between variables

Table 11. Selected independent correlations of regional series (linearly detrended; p uses the effective sample size).

Relationship	Scale	r	n	p	Station-level consistency
Precipitation–humidity	Annual	+0.80	47	<0.001	12 of 15 stations significant
Precipitation–humidity	JJA	+0.90	48	<0.001	–
Precipitation–humidity	MAM	+0.53	48	<0.001	–
Temperature–humidity	MAM	−0.54	48	<0.001	negative at 15/15, significant at 13/15
Temperature–humidity	JJA	−0.58	48	<0.001	negative at 15/15, significant at 14/15
Temperature–precipitation	JJA	−0.49	60	<0.001	negative at 15/15, significant at 14/15
Temperature–precipitation	MAM	−0.30	60	0.02	–
Temperature–precipitation	Annual	−0.25	58	0.06	–
Humidity–PET (Thornthwaite)	Annual	−0.61	48	<0.001	independent of PET method
Humidity–SPEI-12	Annual	+0.80	47	<0.001	–
Winter precipitation–spring humidity	DJF → MAM	+0.34	48	0.02	–
Winter precipitation–SPEI-6	DJF → Apr–Sep	+0.33	59	0.01	–
Winter precipitation–SPEI-12	DJF → annual	+0.38	57	0.004	–

Structural pairs (e.g., P with P − PET, SPEI with SPI, T with Thornthwaite PET) are omitted because they share a component by construction.

Detrended correlations indicate a consistent moisture–heat coupling (Table 11, Figs. 15 and 16). Precipitation and relative humidity co-vary strongly (r = +0.80 annually and +0.90 in summer, n = 47–48; significant at 12 of 15 stations),

and spring and summer temperature are negatively related to humidity (r = −0.54 in MAM and −0.58 in JJA) and, in summer, to precipitation (−0.49) at 14–15 of 15 stations. Annual means weaken these relationships (T–P −0.25, p = 0.059; T–RH −0.28, p = 0.060) because the seasonal signals partly cancel, and in winter there is no temperature–precipitation relationship (r = +0.06). Humidity is also negatively related to Thornthwaite PET (r = −0.61), a relationship independent of the PET formulation because Thornthwaite does not use humidity, and positively to SPEI-12 (+0.80). Winter precipitation shows weak positive lagged relationships with spring humidity (r = +0.34, p = 0.018), April–September SPEI-6 (+0.33, p = 0.012) and annual SPEI-12 (+0.38, p = 0.004), compatible with a snow-pack and soil-moisture memory (a hypothesis not tested here). The share of stations in drought is strongly related to precipitation (r = −0.81) and weakly to temperature (+0.27, p = 0.039, partly structural).

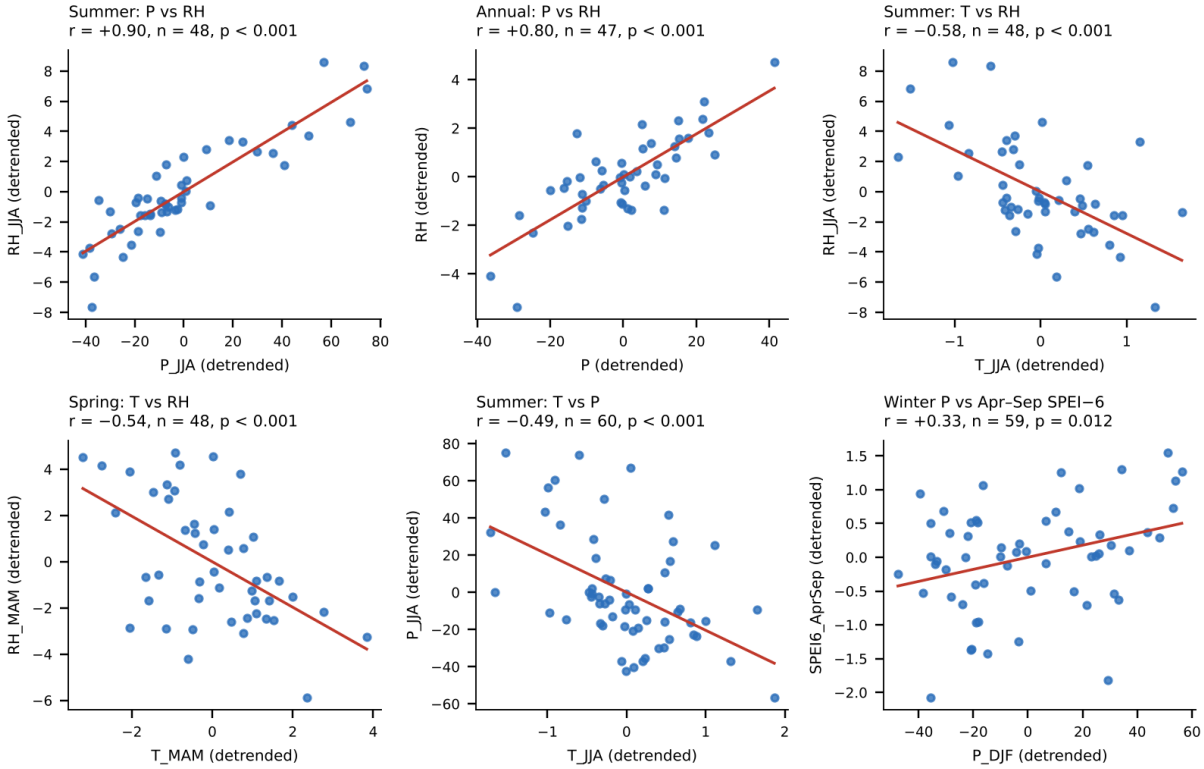

Fig. 15. Scatter plots of detrended regional series for the main independent relationships (line: OLS fit; r, sample size and p based on the effective sample size).

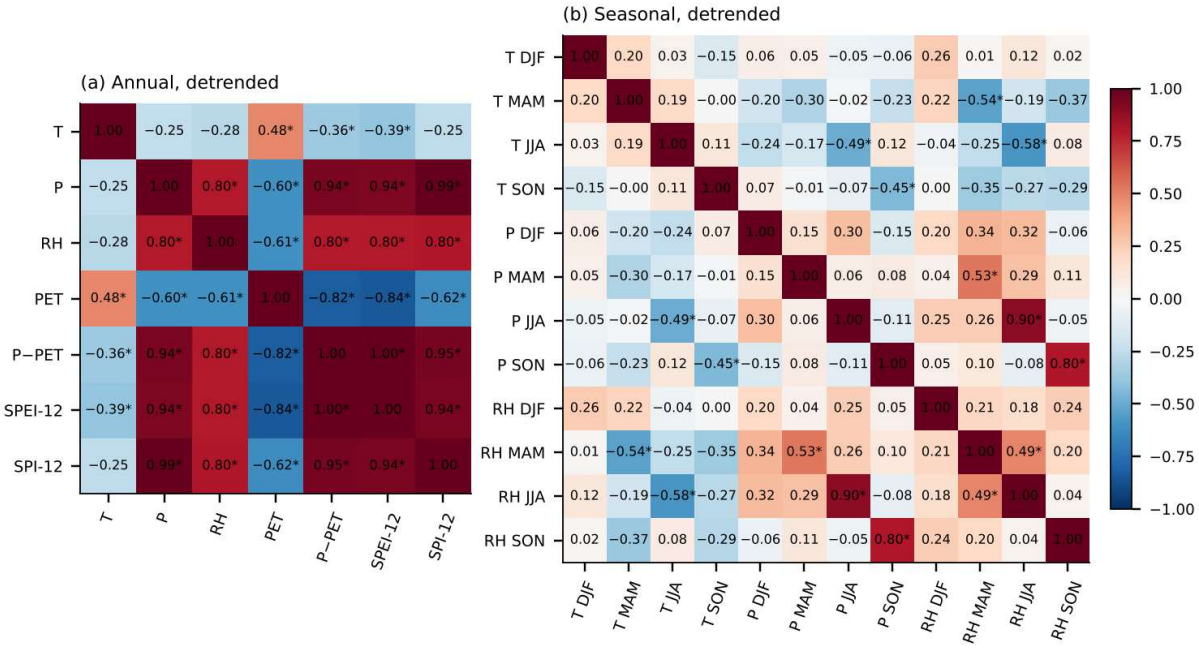

Fig. 16. Correlation matrices of detrended regional series: (a) annual variables including PET, climatic water balance D = P − PET, SPEI-12 and SPI-12 (several pairs are structural by construction), (b) seasonal temperature, precipitation and humidity. Asterisks: BH-FDR q < 0.05.

3.7 Spatial structure of climate fields and interpolation accuracy

Spatial coherence differs sharply by variable (Fig. 17a, Table 12). Temperature anomalies are nearly uniform across the region ($r \geq 0.78$ for all 105 station pairs; median $r = 0.97$ for pairs closer than 150 km and 0.86 for 300–600 km); the decorrelation length of temperature cannot be identified because correlation decays too little within the 569 km extent of the network. In contrast, precipitation decorrelates over 332 ± 36 km ($r = 0.74$ at 100 km and 0.47 at 250 km) and relative humidity over 189 ± 38 km ($r = 0.59$ at 100 km and 0.27 at 250 km). The mean nearest-neighbour distance of the network is 96 km (range 36–181 km) and the mean distance between stations 261 km, so 15 stations are ample for temperature, adequate for regional precipitation and the minimum for humidity, which should not be mapped at finer scales than the station spacing. Differences in elevation between stations do not reduce coherence beyond the effect of distance (partial Mantel $p = 0.20$ for P, 0.56 for RH; for T $p = 0.047$ with a positive sign, i.e. opposite to a physical elevation effect).

Mean climate depends on geography only weakly within the sampled range (Table 12, Fig. 18). Mean annual temperature is unrelated to elevation alone ($\rho = -0.02$) and, with latitude held constant, the elevation coefficient (-3.1 °C km^{-1}, 95% CI -6.9 to $+0.8$) is not distinguishable from zero for the annual mean, while latitude is significant (-0.83 °C per degree; partial $r = -0.68$, $p = 0.007$). In the warm months (April–May, July–October) the elevation coefficient is significantly negative (-4.1 to -4.9 °C km^{-1}); the elevation range of 148–842 m and its collinearity with latitude limit these estimates and they must not be extrapolated to the Tarbagatai, which is described separately with ERA5-Land (Section 3.8). Mean relative humidity decreases with elevation ($\rho = -0.73$, $p = 0.002$, $q = 0.029$), the only mean-climate relationship that survives FDR control. Winter precipitation is lower at higher stations (-9.6 mm per 100 m, CI -18.7 to -0.5), but this reflects the dry south-west (-17 mm per degree of latitude) rather than an orographic effect, which the network cannot test. Trends are not related to geography: the relations between trends and elevation, latitude and longitude all have $q \geq 0.24$. Two relations between trends are noteworthy: stations with larger warming tend to lose more humidity ($\rho = -0.61$, $p = 0.015$, $q = 0.059$; Fig. 18c), subject to the humidity inhomogeneities, and the spatial pattern of SPEI-6 trends follows the precipitation trend ($\rho = +0.75$, $q = 0.008$) rather than the PET trend, because PET increases are nearly uniform.

Table 12. Spatial coherence and geographic controls across the 15 stations.

Test	Result	Interpretation
Decorrelation length L (km)	T: not identifiable ($r \geq 0.78$ for all pairs, 36–569 km); P: 332 ± 36; RH: 189 ± 38	median r (T) = 0.97 below 150 km, 0.86 at 300–600 km; r at 100 km = 0.74 (P), 0.59 (RH)
Partial Mantel, |Δelevation| | distance	T $p = 0.047$ (+); P $p = 0.20$; RH $p = 0.56$	elevation does not reduce coherence
Mean T vs elevation, latitude held constant	-3.05 °C km^{-1} (-6.9 … $+0.8$)	n.s.; latitude -0.83 °C/° ($p = 0.007$)
Mean T vs elevation, warm months (Apr, May, Jul–Oct)	-4.1 … -4.9 °C km^{-1}	CI excludes 0; range 148–842 m only
Mean RH vs elevation	$\rho = -0.73$ ($p = 0.002$; $q = 0.029$)	significant after FDR
Winter P vs elevation (latitude held constant)	-9.6 mm per 100 m (-18.7 … -0.5)	confounded with latitude (-17 mm/°)
Trends vs elevation, latitude, longitude	all $q \geq 0.24$	no geographic control of trends
ρ(trend T, trend RH)	-0.61 ($p = 0.015$; $q = 0.059$)	marginal; RH breaks
ρ(trend P, trend SPEI-6)	$+0.75$ ($q = 0.008$)	pattern follows precipitation

Cross-validated interpolation skill confirms that relief information helps for mean climate but not for trends (Table 13, Fig. 17c). For mean annual temperature, regression kriging on elevation and latitude achieves a leave-one-out RMSE of 1.11 °C, 18% lower than ordinary kriging (1.35 °C), 17% lower than IDW (1.33 °C) and 21% lower than the constant station mean (1.41 °C), a skill of +38%; ordinary kriging, which ignores elevation, has the lowest skill of the spatially explicit methods (+8%). The gain comes from the elevation and latitude drift (OLS alone: 1.15 °C), because the residual field has no useful spatial correlation structure at these distances. For trend magnitudes, in contrast, every method has negative or null skill relative to a constant mean (e.g. raw-slope RMSE 0.0087 °C yr^{-1} for regression kriging versus 0.0074 for the constant), so mapping trend fields by interpolation would add no information beyond the regional mean, which is one reason for presenting trends as station values (Fig. 7).

Table 13. Leave-one-out cross-validation of spatial predictors across the 15 stations.

Predictor	RMSE mean T (°C)	MAE mean T (°C)	Skill vs constant (mean T)	RMSE raw trend (10^{-3} °C/yr)	RMSE adjusted trend (10^{-3} °C/yr)
Constant station mean	1.41	1.00	0	7.42	1.27
Inverse-distance weighting	1.33	1.03	+0.11	8.02	1.37
OLS (elevation, latitude)	1.15	0.85	+0.33	8.76	1.39
Ordinary kriging	1.35	1.12	+0.08	7.47	1.29
Regression kriging (elev., lat.)	1.11	0.89	+0.38	8.74	1.38

Skill = 1 − MSE/MSE(constant mean); positive values mean the predictor is better than assuming the regional mean everywhere. For trend fields all predictors have negative skill.

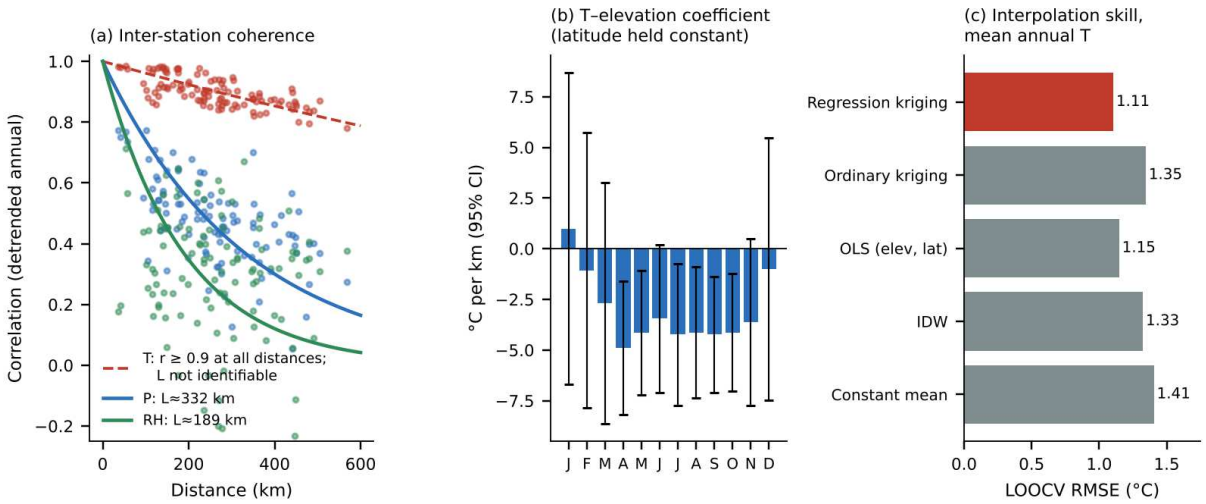

Fig. 17. Spatial structure. (a) Correlation of detrended annual series between station pairs against distance with exponential decorrelation models (L = decorrelation length). (b) Coefficient of elevation in a regression of monthly mean temperature on elevation and latitude (95% CI). (c) Leave-one-out RMSE of spatial predictors for mean annual temperature.

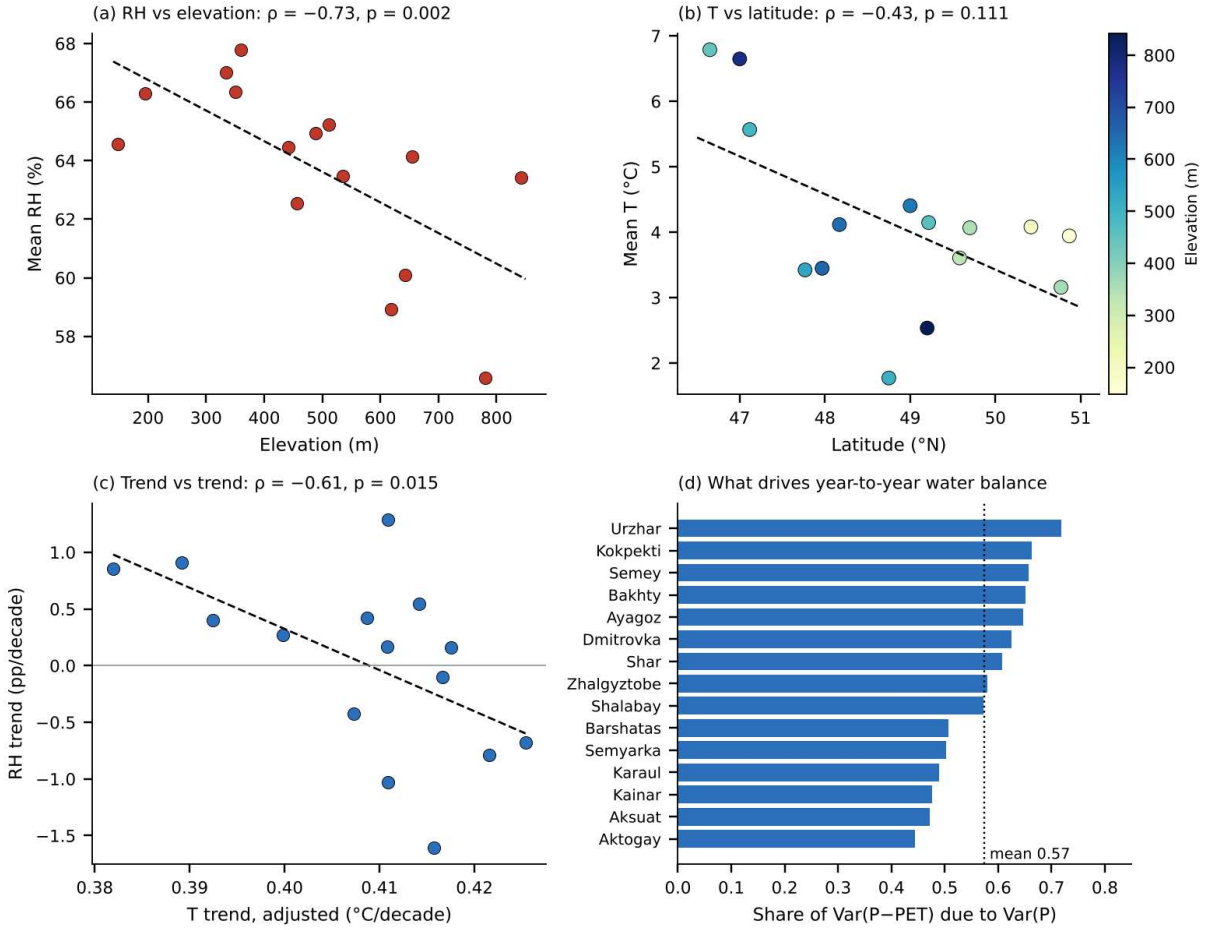

Fig. 18. Geographic controls and drivers of water-balance variability across stations. (a) Mean relative humidity against elevation. (b) Mean temperature against latitude (colour: elevation). (c) Station trends of temperature (adjusted) and relative humidity. (d) Share of the variance of detrended P − PET explained by precipitation variance.

3.8 ERA5-Land validation and climate of the unsampled uplands

ERA5-Land serves here only to describe the uplands: it is first checked against the stations and then summarised by elevation belt. After removal of a regional bias, it reproduces station temperature closely (Table 14, Fig. 19d). The reanalysis is on average 0.61 °C warmer than the stations (mean absolute error 0.70 °C). The interannual correlation of annual temperature is r = 0.71–0.98 (mean 0.93) and the correlation between the regional mean of ERA5-Land and the mean of the 15 stations is 0.95. The bias is seasonal: +1.40 °C in winter against +0.24 to +0.44 °C in the other seasons, while the correlation of seasonal means is highest in winter (r = 0.95) and lowest in autumn (0.90). After adjustment to station elevation the mean bias is +0.62 °C with a station-to-station standard deviation

of 0.64 °C; the largest warm biases are in the east (Kokpekti +1.9 °C; Bakhty, Urzhar, Aksuat +1.2 to +1.3 °C). Subtracting the mean bias, the leave-one-station-out error is 0.54 °C (MAE) and 0.66 °C (RMSE).

Table 14. Validation of ERA5-Land against the 15 stations, 1991–2020 (bilinear interpolation to station coordinates).

Station	Elev. (m)	T station (°C)	T ERA5-L. adj. (°C)	Bias (°C)	r (T)	P station (mm)	P ERA5-L. raw (mm)	P ratio	r (P)
Kainar	842	2.79	2.71	-0.08	0.93	232	368	1.59	0.88
Aktogay	780	6.96	6.70	-0.26	0.89	196	194	0.99	0.60
Ayagoz	655	3.79	4.52	+0.74	0.97	295	353	1.19	0.63
Barshatas	643	4.47	4.82	+0.35	0.94	217	289	1.33	0.64
Karaul	618	4.66	4.21	-0.45	0.91	234	315	1.35	0.70
Aksuat	535	3.83	4.99	+1.16	0.94	214	283	1.32	0.74
Kokpekti	511	2.22	4.10	+1.89	0.93	296	373	1.26	0.73
Urzhar	489	5.57	6.75	+1.18	0.71	456	577	1.27	0.71
Zhalgyztobe	456	4.43	4.54	+0.11	0.95	303	385	1.27	0.65
Bakhty	441	7.03	8.35	+1.31	0.92	308	378	1.23	0.82
Dmitrovka	360	3.44	4.18	+0.75	0.98	332	430	1.30	0.78
Shalabay	350	4.34	4.71	+0.37	0.94	332	445	1.34	0.72
Shar	334	3.83	4.94	+1.11	0.96	291	385	1.32	0.77
Semey	195	4.42	4.95	+0.52	0.97	301	342	1.14	0.72
Semyarka	148	4.24	4.86	+0.62	0.97	221	333	1.51	0.86
Mean / median		4.40	5.02	+0.62	0.93	282	363	1.30	0.73

ERA5-Land temperature was adjusted to station elevation with a lapse rate of −3.1 °C km⁻¹ (Section 2.6); bias = adjusted ERA5-Land minus station; P ratio = ERA5-Land / station mean precipitation (median in the last row). r is the Pearson correlation of annual values (n = 28–30). Station series are not homogeneity-adjusted.

Precipitation is overestimated at 14 of 15 stations (ratio 0.99–1.59, median 1.30; Table 14, Fig. 19e), most strongly in winter (seasonal median ratio 1.55) and least in summer (1.12), a pattern consistent with gauge undercatch of solid precipitation and with a wet bias of the reanalysis, which this comparison cannot separate. The interannual correlation is moderate (r = 0.60–0.88, mean 0.73; seasonal means 0.63 in summer to 0.86 in autumn). Dividing by the median ratio gives a leave-one-station-out mean absolute error of 21 mm (8% of the station mean). The corrected region-wide means are 4.1 °C and 277 mm per year, against 4.40 °C and 281 mm for the mean of the 15 stations (Section 3.4); the agreement for precipitation is partly built in by the scaling.

The corrected fields (Fig. 19a, b) show a warm south (the Zaisan Depression and the Bakhty–Urzhar area) and a cold, wet belt along the Tarbagatai in the south-east that no station samples. In belts of cell-mean elevation (Table 15, Fig. 19c), mean annual temperature falls from 5.3 °C at about 400 m to 1.4 °C above 1,200 m (mean cell elevation 1,540 m), whereas precipitation has a minimum of 252 mm at about 600 m and rises to 468 mm in the highest belt. The highest cell has a mean elevation of 2,433 m, against summit heights of about 3,000 m, so 0.1° cells smooth the relief and the highest belt is underestimated in elevation and probably in extremes. The corrections were calibrated at 148–842 m; the two highest belts (cells above 900 m, 252 of the 2,282 cells) lie beyond the station elevation range, so they are extrapolations that no station can verify.

Table 15. ERA5-Land climate of the Abai Region by belt of cell-mean elevation, 1991–2020 (bias-corrected).

Elevation belt (m)	Cells	Mean elevation (m)	T (°C)	P, corrected (mm)	T trend, ERA5-Land (°C per decade)
< 300	277	231	4.1	278	0.27
300–500	641	405	5.3	268	0.39
500–700	598	604	4.4	252	0.43
700–900	514	789	3.1	272	0.44
900–1,200	171	993	2.6	326	0.44
> 1,200	81	1539	1.4	468	0.44

Cells are 0.1° cells inside the regional boundary. T has the mean bias removed and P is divided by 1.30 (Section 2.6). Values above 900 m lie beyond the station elevation range and are extrapolations.

Trends of the reanalysis disagree with the stations. Over 1991–2020 the regional ERA5-Land temperature rises by +0.41 °C per decade (p = 0.07), twice the +0.19 °C of the mean of the stations (p = 0.36), exceeds the station trend at 13 of 15 stations, and the station-by-station trends are unrelated (r = 0.11; Fig. 19f). The cell trends are spatially uniform (0.19–0.62 °C per decade, median 0.42) and nearly identical in all belts above 300 m (0.39–0.44 °C per decade; Table 15). The regional precipitation trend is +0.9 mm per decade in ERA5-Land (p = 0.92) and +16 mm per decade for the stations (p = 0.14). Neither short-window trend is significant, the station values are not homogeneity-adjusted, and the reasons for the discrepancy were not resolved; ERA5-Land trends are therefore reported only as a comparison and are not used for inference.

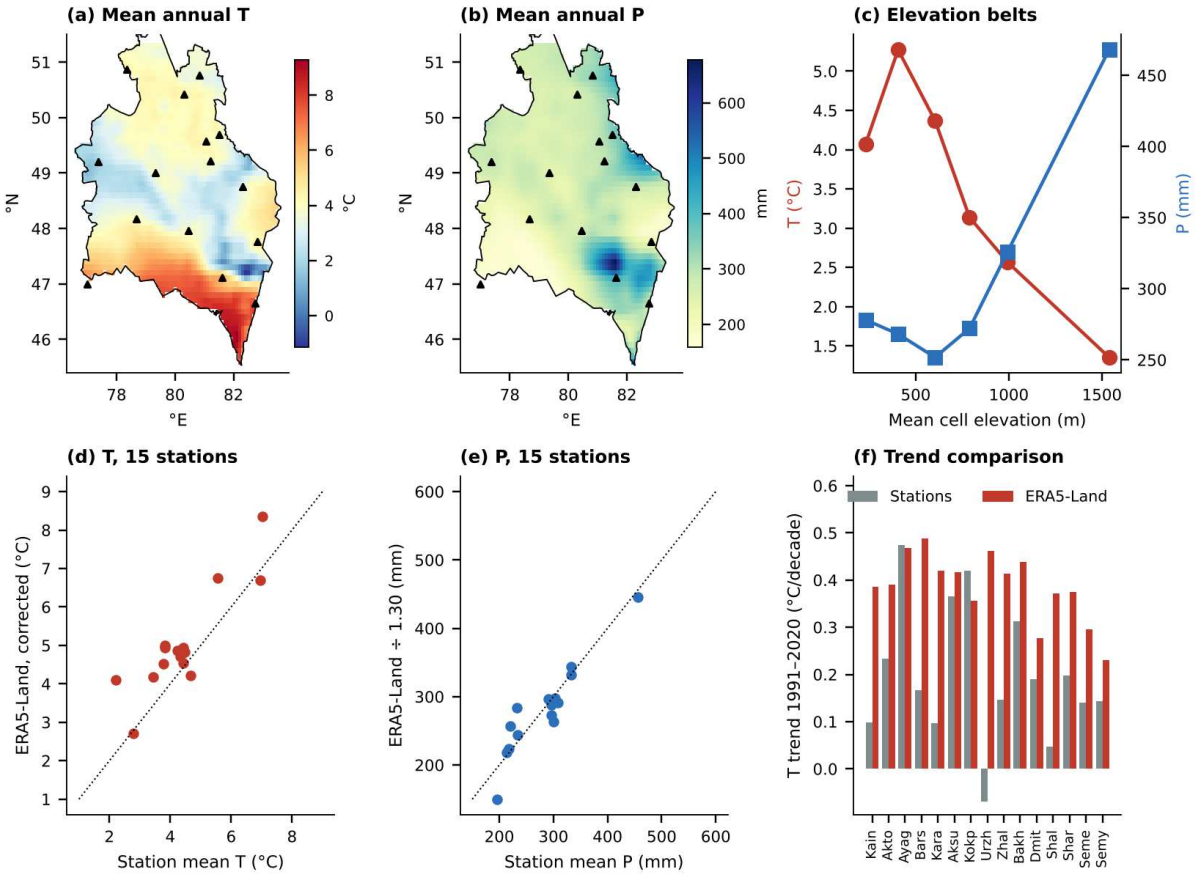

Fig. 19. ERA5-Land, 1991–2020. (a) Mean annual temperature (bias-corrected) and (b) mean annual precipitation (divided by 1.30) inside the regional boundary, with the 15 stations (triangles). (c) Temperature and precipitation by belt of cell-mean elevation. (d, e) Validation against station means: temperature after elevation adjustment, precipitation raw (line: 1:1). (f) Temperature trend 1991–2020 at the stations and in ERA5-Land at the station locations, stations ordered by elevation (high to low).

4. Discussion

4.1 Robust warming, intensified in spring

The Abai Region warmed by +0.41 °C per decade, a rate that exceeds the global-mean surface warming over the same period (IPCC, 2023b) and matches or exceeds earlier reports for Central Asia and Kazakhstan (Bissenbayeva et al., 2025; Broomandi et al., 2025; Haag et al., 2019; Hu et al., 2014; Salnikov et al., 2023). Unlike many earlier station-based estimates, the warming survives break adjustment, serial-correlation control and FDR correction, and it is significant at every station. The step-like character of the change coincides with the well-documented late-1980s regime shift in the Northern Hemisphere (Reid et al., 2016); because circulation indices were not analysed, the timing attribution remains a hypothesis (Section 4.4).

Two points depart from the usual narrative. First, the apparent differences in warming among stations are largely an artefact of inhomogeneous records: after adjustment the rates are statistically indistinguishable and unrelated to elevation, latitude or longitude, so interpolating raw station trends would have mapped instrument changes rather than climate, and no physiographic control on warming is supported within the sampled elevation range. Second, elevation-dependent warming (Aizen et al., 1997; Pepin et al., 2015) cannot be tested here, because no station exceeds 842 m while the relevant gradients occur above 2,000–3,000 m; the absence of an elevation signal applies only to the foothill and steppe belt. ERA5-Land trends are nearly identical in all belts above 300 m (0.39–0.44 °C per decade; Table 15), but because the reanalysis overstates the station trend by about a factor of two (Section 3.8), this cannot be taken as evidence for or against elevation-dependent warming. The seasonal asymmetry is the more distinctive result. Because spring warming coincides with declining spring humidity and precipitation tendencies, snow-cover and soil-moisture feedbacks and earlier snowmelt are plausible contributors (Gong & Ho, 2002; Lioubimtseva & Henebry, 2009), but these were not evaluated.

4.2 Spring and growing-season drying without a precipitation trend

Our central result is that the drying is driven by evaporative demand rather than by rainfall. The SPI does not change, whereas the SPEI declines in spring and in the April–September growing season, while precipitation is statistically stationary in both mean and variability and temperature-based PET rises at all 15 stations. This matches the global finding that warming increases drought hazard through PET even where precipitation is unchanged (Ryssaliyeva et al., 2025; Sheffield et al., 2012; Trenberth et al., 2014). Recent aridity-index analyses for central Kazakhstan likewise report an expansion of arid zones since 1991 (Bissenbayeva et al., 2025). The two controls play distinct roles: precipitation sets the year-to-year severity (wet years are cool and humid), whereas temperature sets the long-term drift.

The size of the drying, however, depends on the PET formulation, a well-known issue (Sheffield et al., 2012). Thornthwaite PET attributes all evaporative-demand change to temperature and underestimates Penman–Monteith by about 27%; the TH-adj. series corrects the level but not this property (its factors are fitted on 2001–2024 and applied unchanged to 1966–2000), and the short Penman–Monteith record shows a smaller, non-significant increase. We therefore regard the SPEI-3 and SPEI-6 declines (−0.18 to −0.21 per decade) as an upper-range estimate of potential drying, and rely on the features that hold across PET choices: the negative sign at all stations, the spring and growing-season seasonality, and the SPI–SPEI contrast. The annual-scale deficit trend is marginal and is treated as such. A full Penman–Monteith SPEI for 1966–2025 would require daily extreme temperature, radiation and wind data for 1966–2000, which were not available.

4.3 Humidity fragility, network adequacy and trend mapping

Relative humidity is the variable most affected by observing practice. Its breaks cluster in 1996–1998 and 2005–2006 with steps larger than the trends of interest, and three of the four stations with significant annual trends carry a detected break. Station-level humidity trends should therefore not be interpreted physically without metadata. The spring decline is more credible, because it is corroborated by independent evidence (faster spring warming, negative T–RH and RH–PET relationships, and falling SPEI) and it persists at stations without breaks. Full-period humidity trends cannot be estimated for six stations, which have no record before 1977; the common period 1978–2025 is therefore used throughout.

The coherence analysis shows that the network resolves regional temperature signals but not sub-regional precipitation or humidity structure: decorrelation lengths of ≈330 km and ≈190 km compare with a mean nearest-neighbour distance of 96 km. Elevation-aware regression kriging improves the mean temperature field, confirming that relief should enter the interpolation (Hengl et al., 2007), whereas no predictor has skill for trend magnitudes. Interpolated trend surfaces, and sign-based response regimes built from non-significant slopes, would visualise measurement noise; trends are therefore shown at station locations (Fig. 7). Interpolating station normals above 842 m would be extrapolation and was not attempted; instead, the uplands are described with ERA5-Land (Muñoz-Sabater et al., 2021), validated against the stations in Section 3.8 (r = 0.93 and a +0.6 °C bias for temperature; a 30% overestimate of precipitation). Because the validation covers only 148–842 m, the belts above 900 m in Table 15 are model-based, and the reanalysis trends, twice the station trends, were not used. A comparison with CHIRPS (Funk et al., 2015) and other gridded products remains to be done.

4.4 Drivers, exposure and implications

The late-1980s step, the dominance of spring warming and the coupling between winter precipitation and the following growing-season SPEI (r = +0.33 to +0.38) suggest, but do not prove, a role for large-scale circulation such as the Siberian High, the Arctic and North Atlantic Oscillations and ENSO (Akhmetkal et al., 2026; Gong & Ho, 2002; Schiemann et al., 2008). Because teleconnection indices were not analysed, these are hypotheses to be tested with the detrended seasonal series provided here, mainly for DJF and MAM.

The analysis quantifies climatic exposure—warming, evaporative demand, humidity and drought frequency—not vulnerability, which additionally depends on sensitivity (crop and pasture type, soils, irrigation) and adaptive capacity. A complementary assessment of agricultural landscape sustainability can be based on the integrated evaluation of climatic, soil, land, biological and water-resource indicators, as demonstrated by a multi-criteria framework using Harrington's generalized desirability function (Omarov et al., 2026). Exposure matters because 87% of agricultural land is pasture (CLRM, 2025), whose productivity depends on spring and early-summer moisture, and because the economy is dominated by primary production (BNS, 2025). Three aspects are actionable: (I) the hazard is seasonal, so drought monitoring should use SPEI-3 for spring and SPEI-6 for April–September rather than annual precipitation; (II) the drift arises from heat and evaporative demand and will continue under further warming irrespective of precipitation changes (Xu et al., 2021); and (III) winter (snow) precipitation is a modest early indicator of growing-season conditions. Because the share of station-months in moderate drought has nearly doubled while extreme drought has not, adaptation should target recurrent moderate conditions (grazing management, early-season water storage, drought-tolerant crop calendars) rather than single-event responses (Karatayev et al., 2022).

4.5 Novelty, widely repeated claims and limitations

The study contributes to the regional literature in four ways: (I) a homogeneity-tested, autocorrelation-aware and FDR-controlled 60-year assessment of three variables for the newly established Abai Region; (II) a demonstration that station differences in warming rates and humidity trends are largely attributable to inhomogeneities, and that trend fields from 15 stations lack spatial structure; (III) a separation of precipitation-driven and evaporation-driven drying through the SPI–SPEI contrast with a transparent PET bracket; and (IV) a quantified test of widely used statements about amplitude of precipitation anomalies, physiographic control and water deficit (Table 16).

Table 16. Widely used statements and the evidence of this study.

Statement	Evidence 1966–2025
Warming is spatially coherent at all stations	Supported: 15/15 stations $q \leq 0.003$; 0.38–0.43 °C per decade after adjustment
Strongest warming in lowland/semi-arid areas (physiographic control)	Not supported: station differences vanish after break adjustment; no elevation, latitude or longitude relationship ($\|\rho\| \leq 0.35$)
Humidity trends differ between stations (Kokpekti, Bakhty decline; Aktogay rises)	Partly: Bakhty, Shar, Dmitrovka decline, Aktogay rises ($q < 0.05$) but three of four have breaks; regional annual trend zero; regional spring decline significant
Precipitation anomaly amplitude is increasing	Not supported: SD ratio 1.06, Levene $p = 0.42$; no station significant
Precipitation trends differ regionally (wetting/drying regimes)	Not supported: no station trend significant after FDR; sign pattern is noise
Progressive intensification of climatic water deficit	Supported for spring and April–September (SPEI −0.18 to −0.21 per decade) via evaporative demand; marginal for annual scale; magnitude depends on PET
Droughts have become more frequent	Partly supported: share of station-months in moderate drought ×1.9 (11.3% → 21.6%); regional episodes 3 → 4 over a longer period; extreme drought unchanged
Vulnerability is increasing	Reframed: exposure assessed; vulnerability not quantified
Anomalies are driven by Siberian High, NAO, ENSO	Not tested; stated as hypothesis
Ordinary kriging is adequate for mapping	Superseded: regression kriging improves mean fields (skill +38%); no method skilful for trends

Several limitations remain. (I) No station metadata were available, so breaks are candidates and the temperature adjustment is a sensitivity analysis; humidity series, with weaker reference correlations, may contain undetected breaks. (II) PET is temperature-based over 1966–2000 (TH-adj. is a level adjustment, not a reconstruction) and Penman–Monteith is available only for 2001–2024; SPEI trends are therefore indicative of potential, not actual, water deficit, and no soil-moisture, runoff or vegetation data were used. (III) The elevation range (148–842 m) excludes the high Tarbagatai and Altai ranges, which are represented only by bias-corrected ERA5-Land fields that are extrapolations beyond the station range (Section 3.8). (IV) Precipitation gauge undercatch and snow measurement changes were not examined. (V) ERA5-Land was compared with the stations (Section 3.8), but its precipitation needed a 30% correction, its temperature trend disagrees with the stations and its evaporation was not validated; MODIS land surface temperature and CHIRPS were not compared. (VI) Teleconnection indices were not analysed. (VII) Many tests were run; FDR control addresses the multiplicity of stations within a family, not across the whole study, so results with p-values near 0.05 (for example winter warming, $p = 0.051$) should be read as indicative. Winter and autumn temperature trends are significant at four stations each only before break adjustment (Section 3.2). Future work should obtain metadata and homogenise with additional reference series, extend to Penman–Monteith SPEI with daily data, add soil-moisture and NDVI indicators, test circulation indices, and couple the observations with downscaled projections (Xu et al., 2021).

5. Conclusions

Homogeneity-tested records from 15 stations show that the Abai Region has warmed robustly (+0.41 °C per decade; +2.4 °C in 1966–2025; step change in 1989), with spring warming 2.5 times faster than summer and robust to break adjustment. After adjustment for six inhomogeneous records, all stations warm at statistically indistinguishable rates (0.38–0.43 °C per decade) that are unrelated to elevation (within 148–842 m), latitude or longitude, so published patterns of spatially differentiated warming should be treated with caution. Precipitation has no trend in any season and its variability has not increased, whereas rising temperature-based evaporative demand reduces the climatic water balance (−10 to −17 mm per decade) and produces significant spring and growing-season drying (SPEI-6 −0.18 to −0.21 per decade), while the share of station-months in moderate drought nearly doubled after 1991. Relative humidity declines in spring but its station-level trends are compromised by instrument-related breaks.

The study therefore supports an increasing climatic water deficit only for spring and the growing season, attributes it to evaporative demand, and treats its magnitude as uncertain because of the PET formulation. Spatially, 15 stations resolve temperature but only regional-scale precipitation and humidity; relief-aware regression kriging improves mean temperature fields, but trends are best shown at station locations. ERA5-Land, corrected against the stations, indicates that the uplands above 1,200 m have a mean annual temperature of about 1.4 °C and about 470 mm of precipitation, but these values are model-based extrapolations and the reanalysis trend (+0.41 against +0.19 °C per decade in 1991–2020) does not replace the station trends. These results quantify climatic exposure—not vulnerability—of pastures and rain-fed crops, and they indicate that drought monitoring and adaptation in the Abai Region should focus on spring and early summer and on evaporative demand. Metadata-supported homogenisation, Penman–Monteith SPEI with daily data, circulation analysis and external validation are the next steps.

Funding

This research was funded by the Science Committee of the Ministry of Science and Higher Education of the Republic of Kazakhstan, Grant No. AP 26194635: “Development of landscape support for the organisation of agricultural nature management in the Abai region for the purposes of sustainable development” (2025–2027).

Data availability statement

The monthly station data are held by RSE “Kazhydromet”. The quality-controlled monthly dataset, annual and seasonal series, homogeneity tests, trend, anomaly, PET, SPEI and correlation tables underlying all figures and tables are

provided as supplementary workbooks and are available from the corresponding author on reasonable request. ERA5-Land monthly averaged data (1950 to present) are available from the Copernicus Climate Data Store (https://doi.org/10.24381/cds.68d2bb30); the validation table and elevation-belt summary are provided in the supplementary workbook.

References:

Aizen, V. B., Aizen, E. M., & Melack, J. M. (1997). Climatic and hydrologic changes in the Tien Shan, Central Asia. *Journal of Climate*, *10*(6), 1393–1404. https://doi.org/10.1175/1520-0442(1997)010<1393:CAHCIT>2.0.CO;2

Akhmetkal, M., Alimkulov, S., Makhmudova, L., Talipova, E., Birimbayeva, L., Kulebayev, K., & Alzhanov, O. (2026). Transformation of river runoff and sensitivity of hydrological systems in the arid zone of Kazakhstan in the context of atmospheric circulation patterns. *Water*, *18*(8), Article 940. https://doi.org/10.3390/w18080940

Alexandersson, H. (1986). A homogeneity test applied to precipitation data. *Journal of Climatology*, *6*(6), 661–675. https://doi.org/10.1002/joc.3370060607

Allen, R. G., Pereira, L. S., Raes, D., & Smith, M. (1998). *Crop evapotranspiration: Guidelines for computing crop water requirements* (FAO Irrigation and Drainage Paper 56). Food and Agriculture Organization of the United Nations.

Beguería, S., Vicente-Serrano, S. M., Reig, F., & Latorre, B. (2014). Standardized precipitation evapotranspiration index (SPEI) revisited: Parameter fitting, evapotranspiration models, tools, datasets and drought monitoring. *International Journal of Climatology*, *34*(10), 3001–3023. https://doi.org/10.1002/joc.3887

Benjamini, Y., & Hochberg, Y. (1995). Controlling the false discovery rate: A practical and powerful approach to multiple testing. *Journal of the Royal Statistical Society: Series B (Methodological)*, *57*(1), 289–300. https://doi.org/10.1111/j.2517-6161.1995.tb02031.x

Bissenbayeva, S., Shokparova, D., Abuduwaili, J., Samat, A., Ma, L., & Ge, Y. (2025). Spatiotemporal dynamics of the aridity index in Central Kazakhstan. *Sustainability*, *17*(15), Article 7089. https://doi.org/10.3390/su17157089

Bretherton, C. S., Widmann, M., Dymnikov, V. P., Wallace, J. M., & Bladé, I. (1999). The effective number of spatial degrees of freedom of a time-varying field. *Journal of Climate*, *12*(7), 1990–2007. https://doi.org/10.1175/1520-0442(1999)012<1990:TENOSD>2.0.CO;2

Broomandi, P., Satyanaga, A., Bagheri, M., Hadei, M., Galán-Madruga, D., Fard, A. M., & Kim, J. R. (2025). Extreme temperature events in Kazakhstan and their impacts on public health and energy demand. *Global Challenges*, *9*(2), Article 2400207. https://doi.org/10.1002/gch2.202400207

Bureau of National Statistics of the Agency for Strategic Planning and Reforms of the Republic of Kazakhstan. (2025). *Main indicators of socio-economic development of the Abai region*. Retrieved May 10, 2026, from http://stat.gov.kz/ru/region/abay/

Chen, F., Huang, W., Jin, L., Chen, J., & Wang, J. (2011). Spatiotemporal precipitation variations in the arid Central Asia in the context of global warming. *Science China Earth Sciences*, *54*, 1812–1821. https://doi.org/10.1007/s11430-011-4333-8

Chen, Y., Li, W., Deng, H., Fang, G., & Li, Z. (2016). Changes in Central Asia's water tower: Past, present and future. *Scientific Reports*, *6*, Article 35458. https://doi.org/10.1038/srep35458

Chernykh, D., Rakhymbek, K., Biryukov, R., Bondarovich, A., Lubenets, L., & Baiburin, Y. (2025). The calculation and mapping of the moisture indices of the East Kazakhstan Region for the preventive assessment of the climate–hydrological background. *Climate*, *13*(7), Article 142. https://doi.org/10.3390/cli13070142

Committee for Land Resources Management of the Ministry of Agriculture of the Republic of Kazakhstan. (2025). *National report on the state and use of land resources in the Republic of Kazakhstan for 2024*. Ministry of Agriculture of the Republic of Kazakhstan. Retrieved May 9, 2026, from https://www.gov.kz/memleket/entities/land

Dai, A. (2013). Increasing drought under global warming in observations and models. *Nature Climate Change*, *3*, 52–58. https://doi.org/10.1038/nclimate1633

Funk, C., Peterson, P., Landsfeld, M., Pedreros, D., Verdin, J., Shukla, S., Husak, G., Rowland, J., Harrison, L., Hoell, A., & Michaelsen, J. (2015). The climate hazards infrared precipitation with stations – A new environmental record for monitoring extremes. *Scientific Data*, *2*, Article 150066. https://doi.org/10.1038/sdata.2015.66

Gnann, S., Baldwin, J. W., Cuthbert, M. O., Gleeson, T., Schwanghart, W., & Wagener, T. (2025). The influence of topography on the global terrestrial water cycle. *Reviews of Geophysics*, *63*(1), Article e2023RG000810. https://doi.org/10.1029/2023RG000810

Gong, D. Y., & Ho, C. H. (2002). The Siberian High and climate change over middle to high latitude Asia. *Theoretical and Applied Climatology*, *72*, 1–9. https://doi.org/10.1007/s007040200008

Haag, I., Jones, P. D., & Samimi, C. (2019). Central Asia's changing climate: How temperature and precipitation have changed across time, space, and altitude. *Climate*, *7*(10), Article 123. https://doi.org/10.3390/cli7100123

Hamed, K. H. (2008). Trend detection in hydrologic data: The Mann–Kendall trend test under the scaling hypothesis. *Journal of Hydrology*, *349*(3–4), 350–363. https://doi.org/10.1016/j.jhydrol.2007.11.009

Hamed, K. H., & Rao, A. R. (1998). A modified Mann-Kendall trend test for autocorrelated data. *Journal of Hydrology*, *204*(1–4), 182–196. https://doi.org/10.1016/S0022-1694(97)00125-X

Hargreaves, G. H., & Samani, Z. A. (1985). Reference crop evapotranspiration from temperature. *Applied Engineering in Agriculture*, *1*(2), 96–99. https://doi.org/10.13031/2013.26773

Hengl, T., Heuvelink, G. B. M., & Rossiter, D. G. (2007). About regression-kriging: From equations to case studies. *Computers & Geosciences*, *33*(10), 1301–1315. https://doi.org/10.1016/j.cageo.2007.05.001

Hosking, J. R. M. (1990). L-moments: Analysis and estimation of distributions using linear combinations of order statistics. *Journal of the Royal Statistical Society: Series B (Methodological)*, *52*(1), 105–124. https://doi.org/10.1111/j.2517-6161.1990.tb01775.x

Hu, Z., Zhang, C., Hu, Q., & Tian, H. (2014). Temperature changes in Central Asia from 1979 to 2011 based on multiple datasets. *Journal of Climate*, *27*(3), 1143–1167. https://doi.org/10.1175/JCLI-D-13-00064.1

Hu, Z., Zhou, Q., Chen, X., Li, J., Li, Q., Chen, D., & Yin, G. (2017). Variations in annual precipitation in Central Asia. *International Journal of Climatology*, *37*(S1), 157–170. https://doi.org/10.1002/joc.4988

Intergovernmental Panel on Climate Change. (2023a). Asia. In *Climate change 2022: Impacts, adaptation and vulnerability. Contribution of Working Group II to the Sixth Assessment Report of the Intergovernmental Panel on Climate Change* (pp. 1457–1580). Cambridge University Press.

Intergovernmental Panel on Climate Change. (2023b). *Climate change 2021: The physical science basis. Contribution of Working Group I to the Sixth Assessment Report of the Intergovernmental Panel on Climate Change*. Cambridge University Press. https://doi.org/10.1017/9781009157896

Karatayev, M., Clarke, M., Salnikov, V., Bekseitova, R., & Nizamova, M. (2022). Monitoring climate change, drought conditions and wheat production in Eurasia: The case study of Kazakhstan. *Heliyon*, *8*(1), Article e08660. https://doi.org/10.1016/j.heliyon.2022.e08660

Karthe, D., Chalov, S., & Borchardt, D. (2015). Water resources and their management in central Asia in the early twenty first century: Status, challenges and future prospects. *Environmental Earth Sciences*, *73*(2), 487–499. https://doi.org/10.1007/s12665-014-3789-1

Künsch, H. R. (1989). The jackknife and the bootstrap for general stationary observations. *The Annals of Statistics*, *17*(3), 1217–1241. https://doi.org/10.1214/aos/1176347265

Levene, H. (1960). Robust tests for equality of variances. In I. Olkin (Ed.), *Contributions to probability and statistics* (pp. 278–292). Stanford University Press.

Li, G., Chen, H., Xu, M., Zhao, C., Zhong, L., Li, R., & Gao, Y. (2022). Impacts of topographic complexity on modeling moisture transport and precipitation over the Tibetan Plateau in summer. *Advances in Atmospheric Sciences*, *39*(7), 1151–1166. https://doi.org/10.1007/s00376-022-1409-7

Li, J., & Heap, A. D. (2014). Spatial interpolation methods applied in the environmental sciences: A review. *Environmental Modelling & Software*, *53*, 173–189. https://doi.org/10.1016/j.envsoft.2013.12.008

Lioubimtseva, E., & Henebry, G. M. (2009). Climate and environmental change in arid Central Asia: Impacts, vulnerability, and adaptations. *Journal of Arid Environments*, *73*(11), 963–977. https://doi.org/10.1016/j.jaridenv.2009.04.022

Löffler, J., Pape, R., & Wundram, D. (2006). The climatologic significance of topography, altitude and region in high mountains – A survey of oceanic-continental differentiations of the Scandes. *Erdkunde*, *60*(1), 15–24. https://www.jstor.org/stable/25647800

Magnan, A. K., Pörtner, H. O., Duvat, V. K., Garschagen, M., Guinder, V. A., Zommers, Z., Hoegh-Guldberg, O., & Gattuso, J. P. (2021). Estimating the global risk of anthropogenic climate change. *Nature Climate Change*, *11*(10), 879–885. https://doi.org/10.1038/s41558-021-01156-w

Mann, H. B. (1945). Nonparametric tests against trend. *Econometrica*, *13*(3), 245–259. https://doi.org/10.2307/1907187

Mantel, N. (1967). The detection of disease clustering and a generalized regression approach. *Cancer Research*, *27*(2), 209–220.

Masson-Delmotte, V. (2024). The physical science basis of climate change empowering transformations, insights from the IPCC AR6 for a climate research agenda grounded in ethics. *PLOS Climate*, *3*(8), Article e0000451. https://doi.org/10.1371/journal.pclm.0000451

McKee, T. B., Doesken, N. J., & Kleist, J. (1993). The relationship of drought frequency and duration to time scales. In *Proceedings of the 8th Conference on Applied Climatology* (pp. 179–184). American Meteorological Society.

Menne, M. J., Williams, C. N., & Vose, R. S. (2009). The United States Historical Climatology Network monthly temperature data, version 2. *Bulletin of the American Meteorological Society*, *90*(7), 993–1007. https://doi.org/10.1175/2008BAMS2613.1

Middleton, N., & Thomas, D. (Eds.). (1997). *World atlas of desertification* (2nd ed.). UNEP/Arnold.

Muñoz-Sabater, J., Dutra, E., Agustí-Panareda, A., Albergel, C., Arduini, G., Balsamo, G., Boussetta, S., Choulga, M., Harrigan, S., Hersbach, H., Martens, B., Miralles, D. G., Piles, M., Rodríguez-Fernández, N. J., Zsoter, E., Buontempo, C., & Thépaut, J.-N. (2021). ERA5-Land: A state-of-the-art global reanalysis dataset for land applications. *Earth System Science Data*, *13*, 4349–4383. https://doi.org/10.5194/essd-13-4349-2021

Omarov, A., Mustafayev, Z., Skorintseva, I., Aldazhanova, G., Kuderin, A., & Toletayev, A. (2026). A multi-criteria framework for assessing the natural resource potential of agricultural landscapes using Harrington's generalized desirability function. *Environmental Monitoring and Assessment*, *198*(7), Article 773. https://doi.org/10.1007/s10661-026-15609-2

Pepin, N., Bradley, R. S., Diaz, H. F., Baraër, M., Caceres, E. B., Forsythe, N., & Miller, J. R. (2015). Elevation-dependent warming in mountain regions of the world. *Nature Climate Change*, *5*(5), 424–430. https://doi.org/10.1038/nclimate2563

Pettitt, A. N. (1979). A non-parametric approach to the change-point problem. *Journal of the Royal Statistical Society: Series C (Applied Statistics)*, *28*(2), 126–135. https://doi.org/10.2307/2346729

Pongratz, J., Schwingshackl, C., Bultan, S., Obermeier, W., Havermann, F., & Guo, S. (2021). Land use effects on climate: Current state, recent progress, and emerging topics. *Current Climate Change Reports*, *7*(4), 99–120. https://doi.org/10.1007/s40641-021-00178-y

Rakhimova, M., Liu, T., Bissenbayeva, S., Mukanov, Y., Gafforov, K. S., Bekpergenova, Z., & Gulakhmadov, A. (2020). Assessment of the impacts of climate change and human activities on runoff using climate elasticity method and GCM. *Sustainability*, *12*(12), Article 4968. https://doi.org/10.3390/su12124968

Reid, P. C., Hari, R. E., Beaugrand, G., Livingstone, D. M., Marty, C., Straile, D., Barichivich, J., Goberville, E., Adrian, R., Aono, Y., Brown, R., Foster, J., Groisman, P., Hélaouët, P., Hsu, H.-H., Kirby, R., Knight, J., Kraberg, A., Li, J., . . . Zhu, Z. (2016). Global impacts of the 1980s regime shift. *Global Change Biology*, *22*(2), 682–703. https://doi.org/10.1111/gcb.13106

Ryssaliyeva, L., Salnikov, V., Lin, Z., & Raimbekova, Z. (2025). Seasonal sensitivity of drought indices in northern Kazakhstan: A comparative evaluation and selection of optimal indicators. *Sustainability*, *17*(21), Article 9413. https://doi.org/10.3390/su17219413

Salnikov, V., Talanov, Y., Polyakova, S., Assylbekova, A., Kauazov, A., Bultekov, N., Musralinova, G., Kissebayev, D., & Beldeubayev, Y. (2023). An assessment of the present trends in temperature and precipitation extremes in Kazakhstan. *Climate*, *11*(2), Article 33. https://doi.org/10.3390/cli11020033

Schiemann, R., Lüthi, D., Vidale, P. L., & Schär, C. (2008). Precipitation climate of Central Asia. *International Journal of Climatology*, *28*(3), 295–314. https://doi.org/10.1002/joc.1532

Sen, P. K. (1968). Estimates of the regression coefficient based on Kendall's tau. *Journal of the American Statistical Association*, *63*(324), 1379–1389. https://doi.org/10.2307/2285891

Sheffield, J., Wood, E. F., & Roderick, M. L. (2012). Little change in global drought over the past 60 years. *Nature*, *486*, 431–437. https://doi.org/10.1038/nature11575

Tabari, H., Marofi, S., Aeini, A., Talaee, P. H., & Mohammadi, K. (2011). Trend analysis of reference evapotranspiration. *Agricultural and Forest Meteorology*, *151*(2), 128–136. https://doi.org/10.1016/j.agrformet.2010.09.009

Thornthwaite, C. W. (1948). An approach toward a rational classification of climate. *Geographical Review*, *38*(1), 55–94. https://www.jstor.org/stable/210739

Trenberth, K. E., Dai, A., van der Schrier, G., Jones, P. D., Barichivich, J., Briffa, K. R., & Sheffield, J. (2014). Global warming and changes in drought. *Nature Climate Change*, *4*, 17–22. https://doi.org/10.1038/nclimate2067

Vakulchuk, R., Daloz, A. S., Overland, I., Sagbakken, H. F., & Standal, K. (2023). A void in Central Asia research: Climate change. *Central Asian Survey*, *42*(1), 1–20. https://doi.org/10.1080/02634937.2022.2059447

Venema, V. K. C., Mestre, O., Aguilar, E., Auer, I., Guijarro, J. A., Domonkos, P., Vertacnik, G., Szentimrey, T., Stepanek, P., Zahradnicek, P., Viarre, J., Müller-Westermeier, G., Lakatos, M., Williams, C. N., Menne, M. J., Lindau, R., Rasol, D., Rustemeier, E., Kolokythas, K., . . . Brandsma, T. (2012). Benchmarking homogenization algorithms for monthly data. *Climate of the Past*, *8*, 89–115. https://doi.org/10.5194/cp-8-89-2012

Vicente-Serrano, S. M., Beguería, S., & López-Moreno, J. I. (2010). A multiscalar drought index sensitive to global warming: The standardized precipitation evapotranspiration index. *Journal of Climate*, *23*(7), 1696–1718. https://doi.org/10.1175/2009JCLI2909.1

Wilks, D. S. (2016). "The stippling shows statistically significant grid points": How research results are routinely overstated and overinterpreted, and what to do about it. *Bulletin of the American Meteorological Society*, *97*(12), 2263–2273. https://doi.org/10.1175/BAMS-D-15-00267.1

World Meteorological Organization. (2017). *WMO guidelines on the calculation of climate normals* (WMO-No. 1203). World Meteorological Organization.

Xu, Z., Han, Y., Tam, C. Y., Yang, Z. L., & Fu, C. (2021). Bias-corrected CMIP6 global dataset for dynamical downscaling of the historical and future climate (1979–2100). *Scientific Data*, *8*(1), Article 293. https://doi.org/10.1038/s41597-021-01079-3

Yao, J., Chen, Y., Guan, X., Zhao, Y., Chen, J., & Mao, W. (2022). Recent climate and hydrological changes in a mountain–basin system in Xinjiang, China. *Earth-Science Reviews*, *226*, Article 103957. https://doi.org/10.1016/j.earscirev.2022.103957

Yapiyev, V., Ongdas, N., Saidaliyeva, Z., Zhiyenbek, A., Smogulova, T., Baigaliyeva, M., & Prikaziuk, E. (2025). Baseline information and regionalization of the large river basins of Kazakhstan. *Frontiers in Water*, *7*, Article 1601671. https://doi.org/10.3389/frwa.2025.1601671

Yue, S., Pilon, P., & Cavadias, G. (2002). Power of the Mann–Kendall and Spearman's rho tests for detecting monotonic trends in hydrological series. *Journal of Hydrology*, *259*(1–4), 254–271. https://doi.org/10.1016/S0022-1694(01)00594-7